REPORT DOCUMENTATION PAGE

Form Approved
OMB No. 0704-0188

1. AGENCY USE ONLY (Leave blank)	2. REPORT DATE	3. REPORT TYPE AND DATES COVERED
	05/04/95	Final Technical

4. TITLE AND SUBTITLE
Photobiology and Optical Properties of Planktonic and Sea Ice Microalgae in the High Arctic

5. FUNDING NUMBERS

6. AUTHOR(S)
Cornelius W. Sullivan

7. PERFORMING ORGANIZATION NAME(S) AND ADDRESS(ES)
University of Southern California
Department of Biological Sciences

8. PERFORMING ORGANIZATION REPORT NUMBER

9. SPONSORING/MONITORING AGENCY NAME(S) AND ADDRESS(ES)
Joseph Wroblewski, ONR

10. SPONSORING/MONITORING AGENCY REPORT NUMBER

11. SUPPLEMENTARY NOTES
Contract No. N00014-88-K-0187

12a. DISTRIBUTION/AVAILABILITY STATEMENT
Approved for public release: distribution unlimited

12b. DISTRIBUTION CODE

13. ABSTRACT *(Maximum 200 words)*

Time series studies of the spectral irradiance fields beneath multiyear pack ice were conducted in the Eastern Arctic Basin at 82-83°N as part of the Coordinated Eastern Arctic Research Experiment (CEAREX). Particulate matter was collected from the multiyear pack ice as well as first year ice in a refrozen lead. The vertical distribution within the ice and the spectral absorbtion properties of the particulates were determined in order to estimate their contribution to the optical properties of the sea ice.

Among the particulates contained in sea ice detritus was common throughout all portions of the pack ice and was the major light absorbing particulate matter in the ice at the time of the observation. Algal cells and mineral-like particulates also were present, yet they contributed to the light-absorbing properties to a lesser extent than the detritus. During early spring, particulate matter contributed little to the bulk attenuation coefficients of the multiyear ice, however, it was estimated to have a more substantial contribution to the attenuation coefficients of first year ice in a refrozen lead. Results of a single stream multilayer radiative transfer model that simulates concentrations of biogenic particulate matter observed in Arctic sea ice indicates that particulate matter within sea ice plays a substantial role in radiative energy transfer and has the potential to seasonally alter spectral irradiance regimes within the ice covered Arctic ocean.

14. SUBJECT TERMS			15. NUMBER OF PAGES
			16. PRICE CODE
17. SECURITY CLASSIFICATION OF REPORT	18. SECURITY CLASSIFICATION OF THIS PAGE	19. SECURITY CLASSIFICATION OF ABSTRACT	20. LIMITATION OF ABSTRACT
unclassified	unclassified	unclassified	UL

PUBLICATIONS RESULTING FROM ONR SUPPORT

Fritsen, C. H., R. Iturriaga, C. W. Sullivan. 1992. Influence of particlate matter on spectral irradiance fields and energy transfer in the Eastern Arctic Ocean. Proceedings of the International Society of Optical Engineering, Vol 1750: 527-541.

*Fritsen, C.H., C.W. Sullivan, and R. Iturriaga. 1992. Influence of particulate matter on spatial variability of the spectral irradiance field and energy transfer in the ice covered Eastern Arctic Ocean during early Spring. SPIE Conference, July 19-24, San Diego, CA.

*It is particularly noteworthy that Mr. Christian Fritsen won the Best Student Paper Award Ocean Optics XI for his presentation.

FINAL TECHNICAL REPORT FOR ONR CONTRACT
No. N00014-88-K-0187
to C. W. Sullivan

Photobiology and optical properties of Planktonic and sea ice microalgae in the high arctic

Absorption Properties of Particulates in Arctic Pack Ice and Snow: Influence on Radiative Energy transfer.

Introduction

Observations (Grossi et al, 1987), measurements (e.g. Palmisano et al, 1987; Perovich, 1993), and radiative transfer models (Arrigo, et al 1992; Grenfell, 1992; Wiscombe and Warren, 1982) have shown that particulate material contributes substantially to the optical properties of sea ice and snow.

From anecdotal observations (Gosselin, pers. comm.;) and a number of systematic studies (Pfirman et al, 1989; Reiminetz et al, 1993), it is readily apparent that drifting pack ice within the central Arctic basin contains substantial biogenic and lithogenic particulate loads. The role of sea ice particulates in radiative energy transfer and/or related biologic and thermodynamic processes in these regions remain relativly unknown.

During the 1989 Coordinated Eastern Arctic Experiment (CEAREX), we investigated the vertical distribution and light absorption properties of particulates in Arctic pack ice. Concurrent assessments of the spectral irradiance fields (above and below the ice) were made in order to estimate the effects of the particulate matter on the apparent optical properties of the ice cover. From these analysis, the

realized and potential effects of pack ice particulates on radiative energy transfer are examined.

Materials and Methods:

Study Area and Instrumentation: Irradiance measurements, including: surface downwelling spectral irradiances ($E_d(0+,\lambda)$), surface upwelling spectral irradiances ($E_u(0+,\lambda)$),surface downwelling scalar irradiances ($E_{od}(0+,PAR)$) as photosynthetically available radiation (PAR) (400-700nm), and under-ice downwelling spectral irradiances ($E_d(z,\lambda)$) were made between April 7 to April 22. All spectral measurements were made with a MER1010 spectroradiometer (Biospherical Instruments) with its 10 nm wavebands centered at 410, 441 455, 488, 507, 532, 550, 570, 589, 633, 656, and 694 nm. $E_{od}(0+,PAR)$ was measured with a Biospherical Instruments model QSR-200 Solar Reference Hemispherical Irradiance sensor. Both instruments were calibrated before and following CEAREX 89 experiments at Biospherical labs in San Diego.

Under-ice measurements were accomplished by mooring the spectroradiometer on an 90° articulated arm deployed through a 75 cm diameter hydrohole drilled with a steam heat drill. The instrument was positioned, and leveled, at the ice/water interface approximately 3 m away from the hydrohole which was covered to avoid stray light from reaching the sensor. With the radiometer still in position, the natural snow cover was manually removed from above the radiometer and the bulk

diffuse spectral attenuation coefficients for both the sea ice and snow were calculated according to calculations described below.

Spectral albedos, $\propto(\lambda)$; A series of eight incident and eight upwelling irradiance measurements (spanning a 12 hour period) were made over a 20 cms of snow overlying multi-year ice (MY ice). Surface albedos were calculated as;

$$\propto(\lambda) = \frac{E_u(0+,\lambda)}{E_d(0+,\lambda)}.$$

Diffuse Attenuation Coefficient for Snow, $K_{dsnw}(\lambda)$; The diffuse spectral attenuation coefficient of snow cover $K_{dsnw}(\lambda)$ (m^{-1}) was estimated according to an exponential model describing the attenuation of downwelling irradiances,

$$K_{dsnw}(\lambda) = -\frac{1}{H} * \ln \frac{E_d(+snw,\lambda)}{E_d(-snw,\lambda)}. \quad (1)$$

H is the thickness of the snow in meters, and $E_d(+snw,\lambda)$ and $E_d(-snw,\lambda)$ are the under-ice downwelling spectral irradiances (units, $\mu E\ m^{-2}\ s^{-1}$) with and without snow, respectively.

Diffuse attenuation coefficient for sea ice, $K_{dice}(\lambda)$; The bulk diffuse spectral attenuation coefficient for optically thick sea ice ($K_{dice}(\lambda)$) was approximated from the following relationship:

$$K_{dice}(\lambda) = -\frac{1}{Z} * \ln \frac{E_d(Z,\lambda)}{E_d(0-,\lambda)} \quad (2)$$

(9,10) where Z is the thickness of the ice in meters, $E_d(z,\lambda)$ is the downwelling irradiance at the bottom of the ice and $E_d(0-,\lambda)$ is the downwelling irradiance just below the surface of the ice. $E_d(0-,\lambda)$ cannot be measured directly in sea ice; but was estimated as

$$E_d(0-,\lambda) = E_d(0+,\lambda) * (1- R_o), \quad (3)$$

where R_o is the specular reflection from the sea ice surface which is estimated according to Arrigo et al (1992).

Although the Beers-Lambert model is a derivation of the radiative transfer equation for a purely absorbing medium and snow and ice can have large ratios of scattering to absorption, the calculated $K_d(\lambda)$'s for both the snow and ice are reasonable approximations of the asymptotic attenuation coefficients when optical depths are sufficiently large.

Sample collections; Two study sites (HH1 and HH2) were established in hummocked multi-year (MY) ice where under-ice irradiances were measured and snow samples and ice cores were also obtained. Two additional cores (designated L1 and L2) were obtained from first-year (FY) ice in an undeformed refrozen lead. Ice cores were obtained (using a 7 cm

diameter CRREL core barrel), sectioned, and allowed to melt at 2°C in closed opaque containers. Snow samples were scooped into clean Nalgene jars and allowed to melt at 2°C. Visibly apparent discolorations and isolated pockets (ca. 5 to 10 cm thickness) of dark particulates were observed in several large 75 cm ice cores that were being drilled with a steam heat drill during routine camp operations. Samples from within these pockets were also extracted and allowed to melt in closed opaque containers.

Absorption Efficiencies of Individual Particles, $Q_a(\lambda)$;

Ice and snow meltwater was filtered through Nucleopore filters (0.4 μm pore size) at low pressures (5 mmHg). Particles retained by the filters were immediately transferred to gelatin coated microscope slides (Iturriaga and Siegel, 1989) and kept frozen until analyzed at USC. Absorption efficiency spectra of the individual particles were determined using a universal microscope (Carl Zeiss) equipped with a type 03 photometer interfaced to a tungsten-halogen light source and a scanning monochrometer. A particle's transmission spectra and a transmission spectra of a particle-free area of the gelatin coated slide are measured and the absorption efficiency factor, $Qa(\lambda)$, is calculated as the difference normalized to the blank measurement. The system is capable of targeting individual microscopic particles with a lower size limit of ~3 μm spherical diameter (additional details are in Iturriaga and Siegel, 1989).

Particulate Absorption Coefficients, $a_p(\lambda)$; Meltwater from sea ice was filtered through glass fiber filters (GF/f). Filters were frozen and transported to USC where spectral absorption coefficients of the bulk particulates ($a_p(\lambda)$) were measured in a double beam spectrophotometer (Uvikon-860, Kontron Instr.) utilizing a filter pad method (Truper and Yentsch, 1967; Mitchell and Keifer, 1988). Scans of the optical densities of sample filters (OD_s) were run from 400 to 750 nm (resolution, 1 nm) against a blank GF/f (OD_b) and the absorption coefficients were calculated as

$$a_p(\lambda) = \frac{\ln(10)(OD_s - OD_b)\ A}{V_f \beta}. \qquad (4)$$

A is the clearance are of the filter, V_f is the volume of sample filtered, and β is the pathlength amplification factor (Butler 1962) resulting from scattering within the filters. β was modeled according to Bricaud and Stramski (1990).

Estimates of the particulate's effect on irradiance transmission, $E_d(Z,\lambda)$, To evaluate the particulate's effects on the apparent optical properties of the ice it is necessary to extrapolate the measured inherent absorption properties of the particulates (Q_a's and a_p's) to apparent absorption properties. Vertically averaged absorption coefficients $\langle a_p(\lambda) \rangle$ can be calculated as,

$$\langle a_p(\lambda) \rangle = \frac{\Sigma a_p(\lambda)_n * Z_n}{Z} \quad (5)$$

where $a_p(\lambda)_n$ (m^{-1}) is the particulate absorption coefficient and Z_n (m) is the thickness of each section (n) within an ice core. Dividing $\langle a_p(\lambda) \rangle$ by the mean cosine of the downwelling irradiance stream (μ_d) approximates a vertically averaged particulate attenuation coefficient $\langle K_{dp}(\lambda) \rangle$. μ_d is assumed to be equal to 0.65 to approximate a diffuse radiance distribution within sea ice(Grenfell, 1983; Arrigo et al, 1992). $\langle K_{dp}(\lambda) \rangle$ estimated in this manner represents a weighted average over the entire ice thickness and, therefore, does not rely on or account for vertical variations in particulate concentrations. This approach also neglects the scattering effects of the particles and, therefore, is likely to be a conservative estimate of the particles effects on the ice's apparent optical properties.

The influence of the sea ice particulates on the transmission of irradiances into water column can be calculated and illustrated by subtracting $\langle K_{dp}(\lambda) \rangle$ from the measured sea ice attenuation coefficients and predicting transmitted irradiances for a "particle free" scenario. Converting photon fluxes (units, $\mu E\ m^{-2}\ s^{-1}$) to energy fluxes (units, $W\ m^{-2}$) according to

$$W\ m^{-2} = \mu E\ m^{-2}\ s^{-1} * \frac{hc}{\lambda} \quad (6)$$

(h = Planck's constant, c = speed of light) and integrating the difference between the measured spectra and the predicted particle-free scenario, produces an estimate of the reduction of transmitted energy due to the presence of particulate impurities. A similar analysis can be made for first-year ice in the refrozen lead. However, because we were not able to measure attenuation coefficients of the lead ice, we utilize Perovich's (1990) approximations for first-year blue ice and predict transmission spectra with and without the addition of $<K_{dp}(\lambda)>$.

Results:

General observations; Salinities (measured with a Bausch and Lomb refractometer) of the MY ice ranged from 0 ppt near the surface to 15 ppt near the ice water interface -profiles indicative of MY ice undergoing brine drainage. FY ice salinities ranged from 5 to 10 ppt and exhibited a typical "C" shaped profile for FY ice. MY ice cores contained internal bands and isolated pockets of visibly detectable particulates while FY ice appeared particulate-free to unaided eyes.

Individual particulates and their absorption properties: Microscopic observations of particulates collected from both the MY and FY ice revealed a diverse assemblage of particulates including: empty diatom frustules, various species of pigmented pennate diatoms, tetrads of cells of

unknown taxonomic affinity, arthropod remains, flocculant detrital material, minerals, and aggregates containing all of the above mentioned material.

The majority (61%) of the algal cells were pennate diatoms ranging in size from 10 to 80 μm in length. Their $Q_a(\lambda)$ spectra were typical for marine diatoms- having primary and secondary absorption peaks centered at 435 and 670 nm (figure 1A). Within the cold and low-saline upper regions of the MY ice, spherical spores (8 to 20 μm diameter), often found in tetrads, were abundant among an assemblage of empty pennate diatom frustules. Spores had distinct absorption spectra with a very broad primary absorption peak centered at 476 to 480 μm (figure 1A) -indicative of a large compliment of photoprotective and/or accessory pigments. Flagellated microalgae also were present and were relatively more abundant near the bottom of the FY ice but were also found within the visibly discernable bands in the MY ice. Flagellates had primary absorption peaks centered at 435 and 665 μm with a pronounced shoulder at 470 μm (figure 1A) -spectral characteristics indicative of Chlorophyll b absorption (Bidigare et al, 1988)

The majority (70%) of the non-cellular particulates were grayish appearing amorphous aggregates of flocculant material. $Q_a(\lambda)$ were larger at shorter wavelengths and had a monotonic decrease towards the red wavelengths (Figure 1B). This spectral signature is characteristic for marine detritus (Kishino et al, 1984; Roesler et al, 1989; Bricaud and

Stramski, 1990). The remaining 30% of the non-cellular particles were either mineral particulates (identified by angular edges, facets, color, and cross polarization microscopy) or very dense orange appearing amorphous particles. The orange appearing amorphous particulates had very high and relatively constant absorption efficiencies at wavelengths less than 500-515 nm and at wavelengths greater than 500 nm, a monotonic exponential decrease in $Q_a(\lambda)$ (figure 1B). They appeared as dense orange particles when viewed with white light microscopy but they exhibited no other distinguishing features. These particles will be designated as "type ii detritus" in this paper in order to distinguish them from the grayish detrital particles that will be designated as "type i detritus". Several of the mineral particulates (5 to 30 μm) had distinct $Q_a(\lambda)$ spectra having a concave upward signatures (figure 1B). Using cross polarizing microscopy, several of these minerals were identified as biotite particles. Feldspar, quartz, and other transparent clay minerals were also present, but their absorption efficiencies were below levels of detection.

Small, 3 - 20 μm particles of biotite, chlorite, quartz/feldspar, and amorphous soot particulates were also abundant in snow samples examined via cross polarization microscopy. Absorption efficiency spectra were larger at shorter wavelengths with no other apparent distinguishing features (Figure 1C).

Bulk absorption coefficients; Vertical profiles of the absorption coefficients of the bulk particulates collected from the ice cores show that the amorphous type i detritus was optically predominant throughout much of the MY and FY ice (figure 2 A and B). Sections of ice that contained visibly apparent discolorations had increases in the relative contribution of algal pigments to the bulk absorption properties of the particulate matter (detected as a discernable peak at 675 nm). $A_p(\lambda)$s of bulk samples extracted from visible "pockets" of particulates were much larger than those within the ice cores and were dominated by algal pigments (figure 2C). A detrital component was still apparent in these samples - causing the primary absorption peak to be centered at 410 to 420 nm rather than the 435 nm chlorophyll a peak measured for individual algal cells.

Albedo; Albedos above CEAREX's snow cover (figure 3) were measured on April 9th under clear sky conditions. One source of variability is attributable to the effects of differing solar angels during the 12-hour measurement period. The notable features in the albedo are: 1) they are low (0.4-0.5) over all wavelengths and 2) albedos are larger at the longer wavelengths. These features of the albedo are consistent with particulate contaminations.

Ice and Snow Attenuation Coefficients; A $K_{dsnw}(\lambda)$ spectrum is illustrated in figure 4 along with the under-ice irradiance spectra used in its calculation. The removal of the snow cover increased the transmitted energy by four-fold. The $K_{dsnw}(\lambda)$ values are low compared to dry compact snow (Perovich, 1990) but may be reasonable for an ice-snow mixture which was observed at this site. Lower values may also be partly artifactual; because specular reflection from the air/ice interface is not accounted for in equation #1.

Attenuation coefficients for the ice at both of the MY sites were similar in magnitude and spectral shape (figure 5), and fell between those previously reported for "white" and "blue" ice in the Arctic (Grenfell & Maykut, 1977). These coefficients are consistent with the visual observations of the ice cores being comprised of a "white ice" layer ca. 10 cm deep underlain by more visually transparent ice.

Particle's effects on transmitted irradiances; Particulate matter at CEAREX "O" camp was estimated to have had a relatively small influence on photon and energy flux into the water column (Figure 7 A-C). The estimated effect was a reduction of transmitted energy by 20% (0.2 W m^{-2} when incident flux is 300 W m^{-2}) through MY ice and 10% (3 W m^{-2}) through the FY ice. The highly concentrated pockets of material were estimated to cause the largest alterations of the transmitted energy and irradiance spectra (figure 7C).

The estimated effect was to reduce the transmitted energy by 65% (5.5 W m^{-2}) and shift the wavelength maxima from 496 nm to 520-526 nm. This is a comparable effect as those measured and modeled for a microalgal blooms in Arctic bottom ice near the seasonal maxima (Perovich et al, 1993).

Discussion:

Albedo;

The snow's albedo at "O" camp was characteristic of a snow pack contaminated with particulate matter (figure 3). Our microscopic analysis showed the presence of several types of amorphous flocculant and lithogenic particles. The possibility that some of these particulates originated from within the camp cannot be entirely discounted. However, several investigators have found black carbon, minerals, and other particulates within Arctic snow and within the famous "Arctic Haze". Our spectral measurements of their absorbing properties (fig 4c) are consistent with those measured at discrete wavelengths (435, 525, 660 and 880 nm) on different particulate assemblages found throughout the Arctic Basin (Clark and Noone, 1985).

Irradiance Transmission;

As has been demonstrated on multiple occasions, snow cover is a major constituent influencing the transmission of irradiances into and through the ice cover (Grenfell and Maykut, 1975; Perovich, 1990). The snow cover at CEAREX "O"

camp was no exception. The snow cover accounted for an 70-90% reduction of shortwave radiation (400-700nm) passing through MY ice and accounted for an estimated 50-80% reduction of energy passing through FY ice in a refrozen lead (data not shown).

Particulate impurities in the ice also contributed to the reduction of transmitted irradiances (figure 7 A-C). Their effect was much less dramatic than that of the snow cover. However, the magnitude of the particle's effect may be substantial in terms of energy transfer processes under certain conditions. For example, the particle's reduction of short-wave energy flux through the lead under clear skies is of the same magnitude as the mean oceanic heat flux for the central Arctic Ocean (2 W m^{-2}, Maykut and Perovich, 1987).

Absorption efficiency spectra of individual particulates can be utilized in radiative transfer models to elucidate the potential effects different types of particles can on energy transfer processes. The absorption coefficients of the particulate matter can be calculated from the $Q_a(\lambda)$'s as follows:

$$a_p(\lambda) = Q_a(\lambda) * N * g$$

where N is the concentration of particles, and g is their optical cross section (Iturriaga and Siegel, 1989).

Different compliments of particulate loads are predicted to change the spectral quality of transmitted irradiances. For example, the difference between sea ice containing diatoms

versus flagellates at equal cell numbers is a definitive spectral shifting of the wavelength maximum of the transmitted downwelling irradiance spectrum (fig 8a). A detrital-dominated particulate compliment, on the other hand, produces a transmitted downwelling irradiance spectrum with a broad peak but little spectral shifting (fig 8b).

As algorithms are being developed to remotely sense sea ice and snow thicknesses as well as algal standing crops (e.g. Legendre and Gosselin, 1991; Perovich et al, 1993), Q_a spectra may be useful in the algorithm development for the deconvolution of the bulk apparent optical properties into the respective inherent optical properties of the sea-ice constituents.

Particles effects on Primary Production;

Sea ice particulates, in effect, compete with photosynthetic organisms for photons. Photons absorbed by ice, water, soot, biotite, detritus and other non-photosynthetic constituents are no longer available for absorption by algae. Therefore, the initial effects of impurities in ice are to reduce the potential rates of primary production. In sea ice ecosystems and in the underlying water column light absorption is considered to be a rate-limiting ecological process (Grossi et al., 1987). However, if sea ice particulates accelerate ice decay by contributing to a positive feed-back process involving ice deteriation (Eicken et al., 1991) and decreasing ice

concentrations leading acclerated ice decay (Maykut and Perovich, 1987), then water column blooms (and primary production) may be enhanced. The potential positive and negative feebacks process associated with these scenarios make it difficult to predict the effects that particulates have on annual production cycles. However, they undoubtedly play a role in the timing and location of production.

Energy Budgets and Regional Albedos: The absorption of electromagnetic energy by particulates on the surface of the ice and snow has been recognized as an important influence on albedo (this study, Wiscombe and Warren, 1982) and localized energy budgets. If particulates material, both lithogenic and biological are present in the ice over large scales (and there is evidence that thery are) then they are potentially important for local, regional, and, perhaps, global energy budgets.

The potential for discrete bands and pockets of absorbing particulates within the interior sea-ice matrix for altering localized energy transfer processes and regional energy budgets through indirect means is recognized. Internal bands of particulate matter leading to internal heating or melting will, in turn, influence the optical (Grenfell, 1983) and mechanical (Buynitsky, 1968) properties of ice. Therefore, it is likely that internal heating contributes to the positive feedback dynamic that accelerates the decay of a

sea-ice cover. Accelerated opening of ice-free water, in turn, causes lowered regional albedos.

Algal communities on the bottom of FY Arctic ice as well as Antarctic FY ice have been observed to ablate earlier than the surrounding ice due to localized heating effects of the algae (Grossi et al, 1987; Lewis and Cota, unpublished). Cryoconite holes forming on the surface of the ice are another example of particulates having an easily recognizable/identifiable influence on ice dynamics. Internal heating and melting within sea ice, however, will only manifest its effects as alterations of internal sea ice structure and/or accelerations of ice decay at the lower boundary and, therefore, is a phenomena that is less readily observable.

Multiple studies indicate particle-laden pack ice in the Arctic basin is common and is a significant carrier for cross-shelf transport of sediments and continental shelf erosion (Pfirman et al, 1989). The potential significance of particle-laden ice throughout the Arctic basin on energy budgets has been suggested (e.g. Pfirman et al., 1987) and are particularly reinforced by our findings of internal banding and their potential direct and indirect effects of internal heating. Because particulate material in sea ice and snow is variable in both space and time and the pack ice is relatively inaccessible, we can not yet determine- quantitatively- the role internalized particulates have in determining the optical, thermal, and biological properties

of Arctic sea ice on regional scales. Further analysis of the factors controlling the spatial (both vertical and horizontal) and temporal distribution of terrigenous matter, aeolian particulates, detritus, and algae in sea ice seems warranted. Moreover, the development of remote sensing algorithms for detecting particulate loads in ice will be useful tools in understanding the dynamics of polar ecosystems. The presence of several different types of particulates with differing optical characteristics makes the interpretation of existing algorithms (Legendre and Gosselin, 1991; Perovich et al, 1993) problematic.

Figure Legends

Figure 1. Absorption efficiency spectra of: A). diatoms, flagellates and spores found within MY pack ice (Flagellates and diatoms were also common in FY ice samples), B). detrital and mineral particulates found within MY pack ice, and C). snow particulates.

Figure 2. Bulk particulate's absorption coefficients of particles collected from discrete sections of: A) MY ice cores; B) FY ice cores; and C) visibly apparent discolorations within MY ice -illustrated as bands and pockets of dark matter.

Figure 3. Spectral Albedos of Snow. Measured values (mean ± 2 standard errors, n= 8) are those for a X cm metamorphosed snow cover (i.e. firn) at CEAREX "O" camp. Pure snow, 100 ppmw ash, and 1,000 ppmw ash spectra are albedos predicted by Wiscombe and Warren (1982) for varying concentrations (ppm by weight, ppmw) of Mt. St. Helen's ash in a model snow pack with grain radii of 1,000 μm.

Figure 4. A). Downwelling spectral irradiances beneath 2.x meters of MY ice with and without 20 cm's of snow. Incident surface irradiances were 1710-1720 $\mu E\ m^{-2}\ s^{-1}$ and the downwelling irradiance beneath the ice was 0.3 $\mu E\ m^{-2}\ s^{-1}$ (0.073 $W\ m^{-2}$) with snow and 1.39 $\mu E\ m^{-2}\ s^{-1}$ (0.329 $W\ m^{-2}$)

without. B). Diffuse attenuation coefficient for snow (n = 13, Error bars, $\pm$ 2 standard deviations).

Figure 5. Diffuse attenuation coefficients for MY ice at "O" camp. Also shown are attenuation coefficients for "blue" ice and "white" ice (after Grenfell and Maykut, 1975).

Figure 6. Predicted downwelling spectral irradiances beneath: A). MY ice with a 20 cm snow cover with and without <Kp>s calculated for "O" camp MY ice. Predictions suggest that particulates accounted for a 20% reduction (0.5 W m^{-2} less when incident irradiance = 300 W m^{-2}) of transmitted energy; B). FY ice with X cm snow cover with and without <Kp>s of "O" camp FY ice. Particulates account for a reduction of 3.0 W m^{-2} - a 10% reduction of transmitted energy; C). 2.78 m of MY ice with a 10 cm band of particles with aps measured in algal "pockets" (fig. 6c). Energy reduction due to a band of particulates and algae = 5.5 W m^{-2} - a 65% reduction in energy transmission.

Figure 7. Predicted downwelling spectral irradiances beneath ice containing comparable numbers of A). diatoms or flagellates; B). diatoms or detritus.

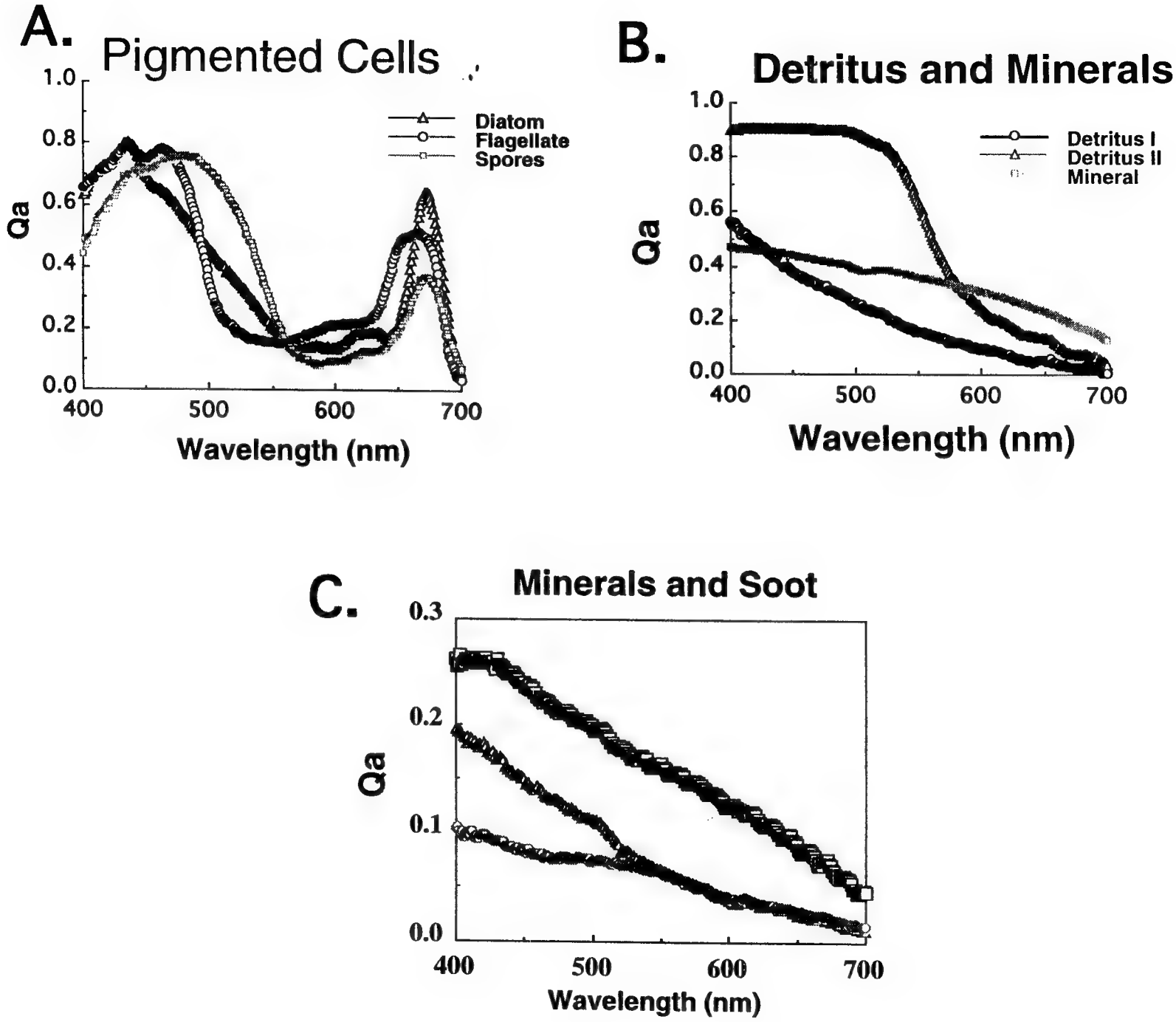
A.
Pigmented Cells
Diatom
Flagellate
Spores
Qa
Wavelength (nm)
B.
Detritus and Minerals
Detritus I
Detritus II
Mineral
Qa
Wavelength (nm)
C.
Minerals and Soot
Qa
Wavelength (nm)

Fig 1 A-C

Fig 2

A

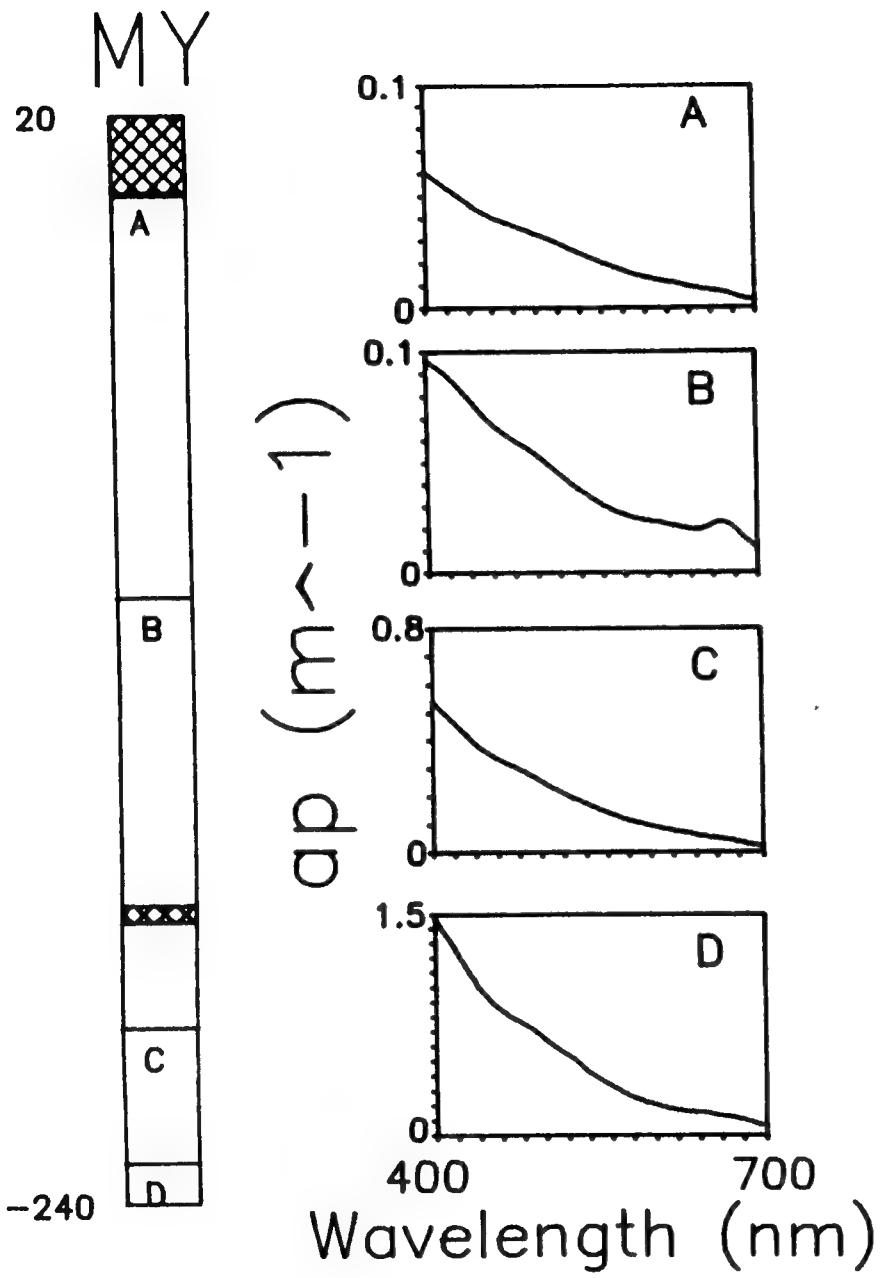
MY
20
A
B
C
D
−240
0.1
A
0
0.1
B
0
0.8
C
0
1.5
D
0
400
700
Wavelength (nm)
ap (m−1)

B

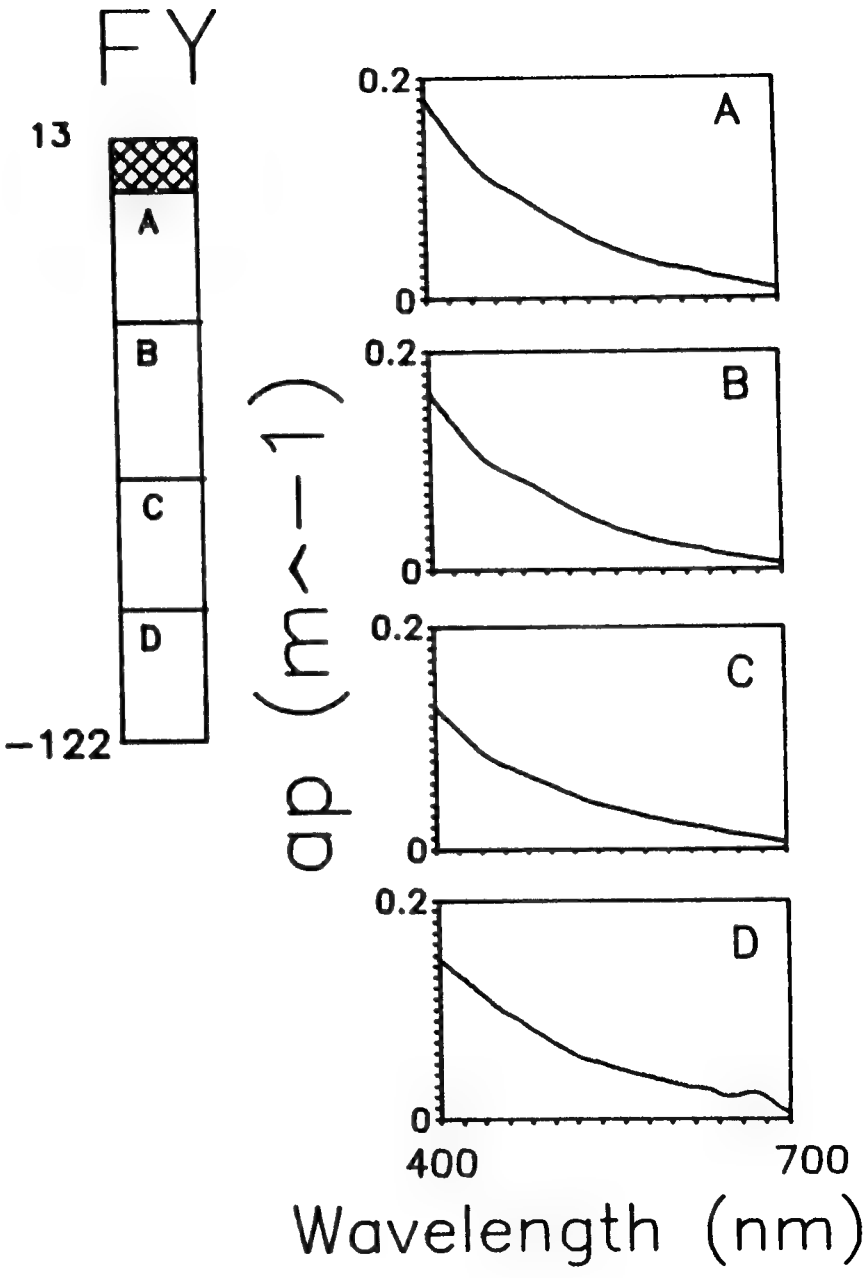
FY
13
A
B
C
D
−122
0.2
A
0
0.2
B
0
0.2
C
0
0.2
D
0
400
700
Wavelength (nm)
ap (m−1)

Fig 2 c

C.

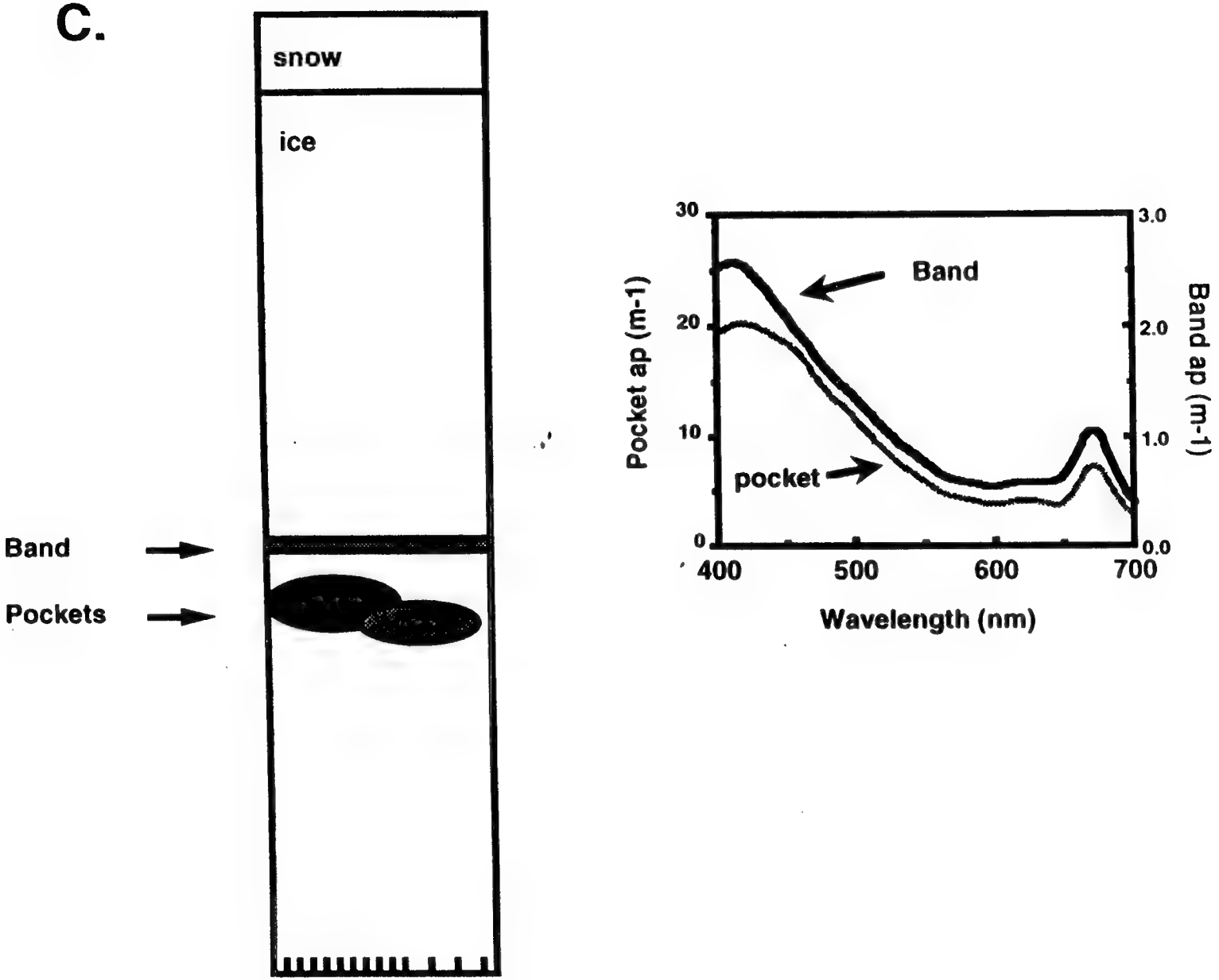
snow
ice
Band
Pockets
30
20
10
0
3.0
2.0
1.0
0.0
Pocket ap (m-1)
Band ap (m-1)
Band
pocket
400
500
600
700
Wavelength (nm)

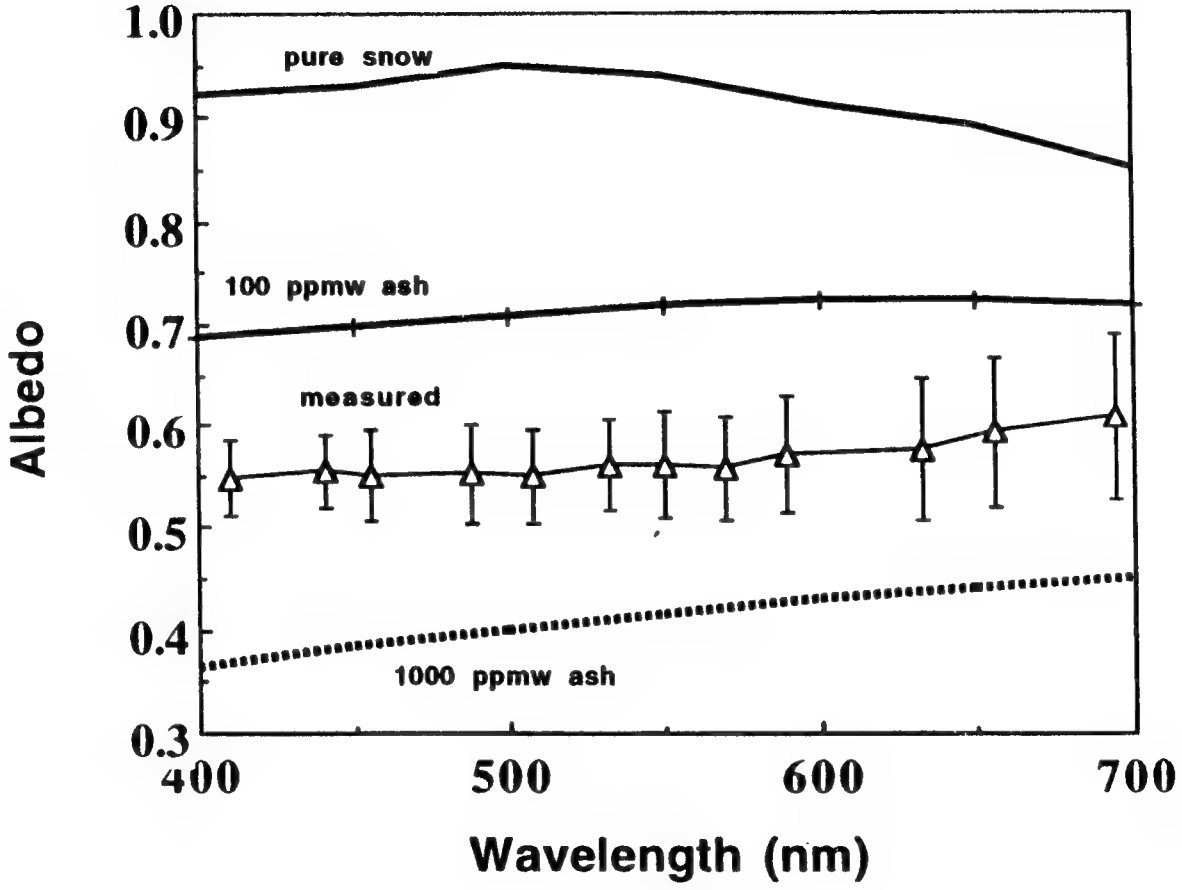
1.0
0.9
0.8
0.7
0.6
0.5
0.4
0.3
Albedo
pure snow
100 ppmw ash
measured
1000 ppmw ash
400
500
600
700
Wavelength (nm)

Fig. 3

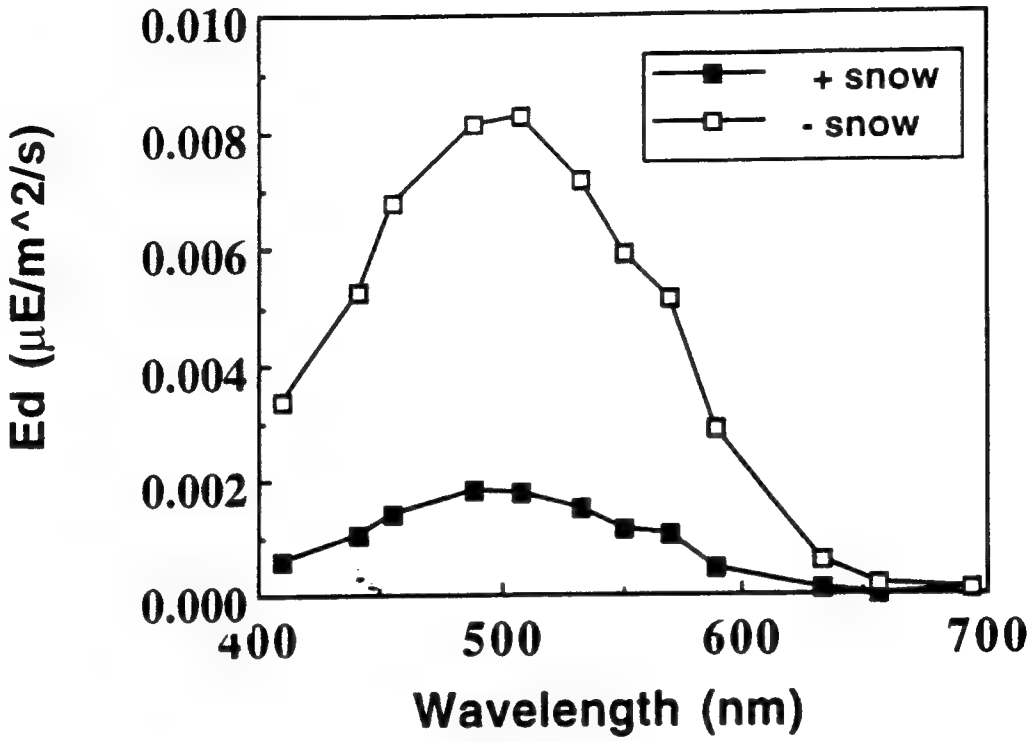
0.010
0.008
0.006
0.004
0.002
0.000
Ed (µE/m^2/s)
+ snow
- snow
400
500
600
700
Wavelength (nm)

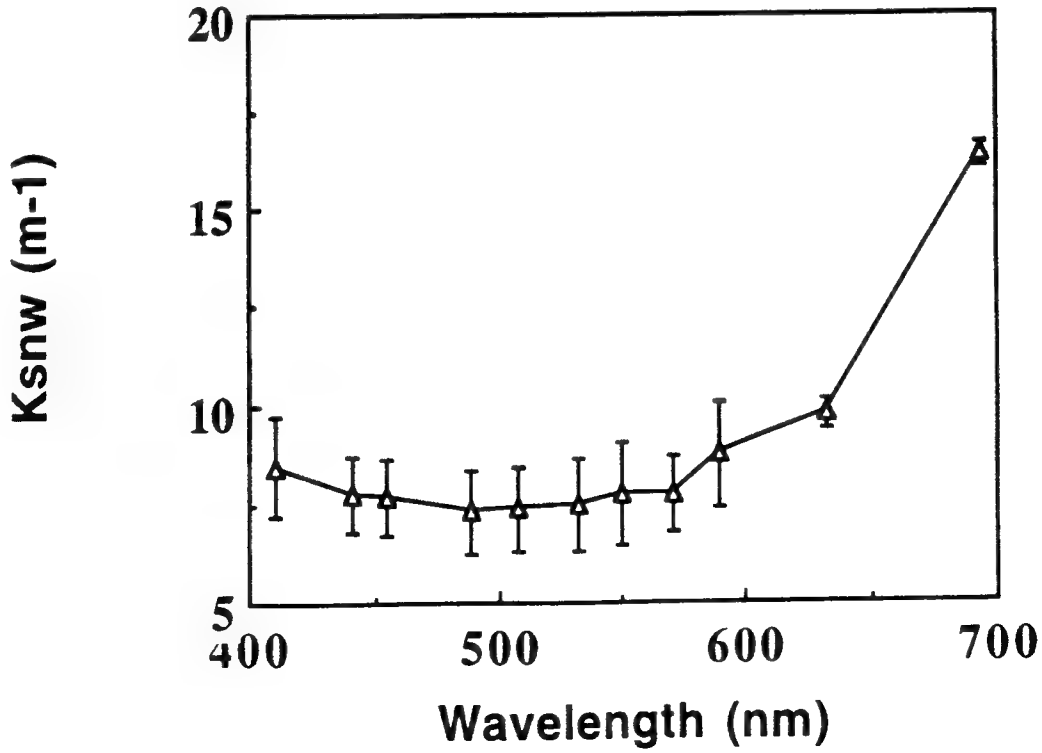
20
15
10
5
Ksnw (m-1)
400
500
600
700
Wavelength (nm)

Fig 4

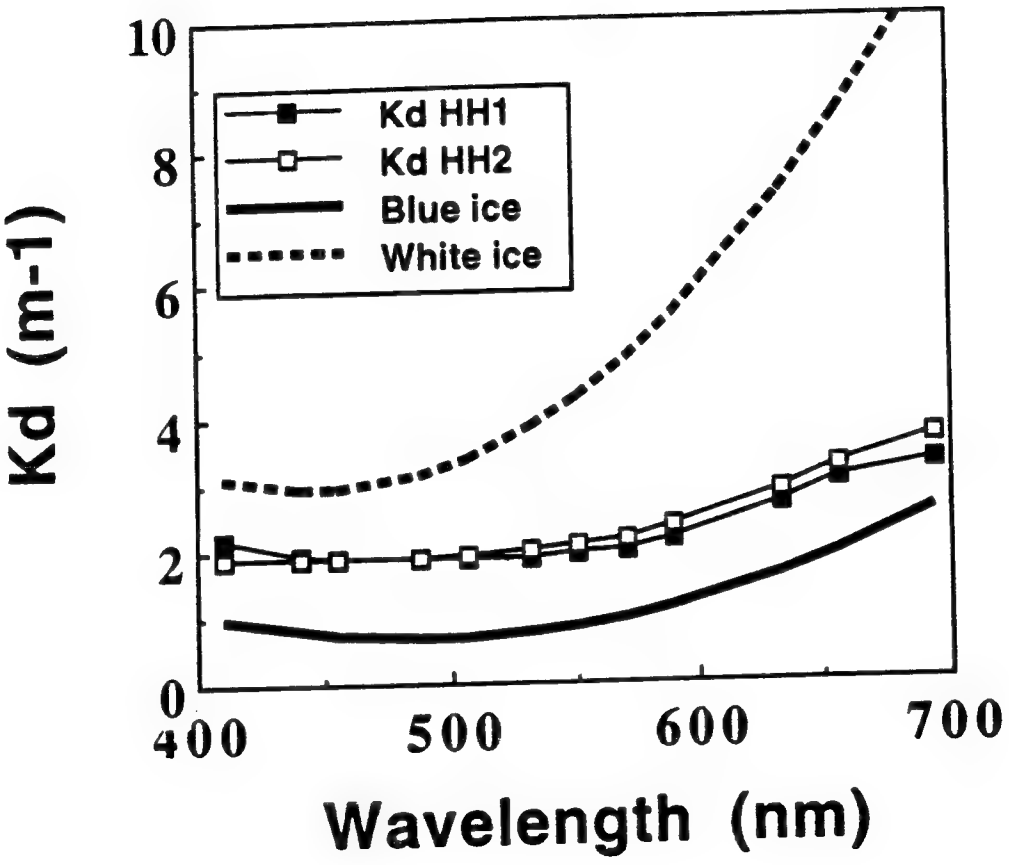
Kd HH1
Kd HH2
Blue ice
White ice
Kd (m-1)
10
8
6
4
2
0
400
500
600
700
Wavelength (nm)

Fig 5

Particle's effect on transmitted irradiances (MULTIYEAR ICE)

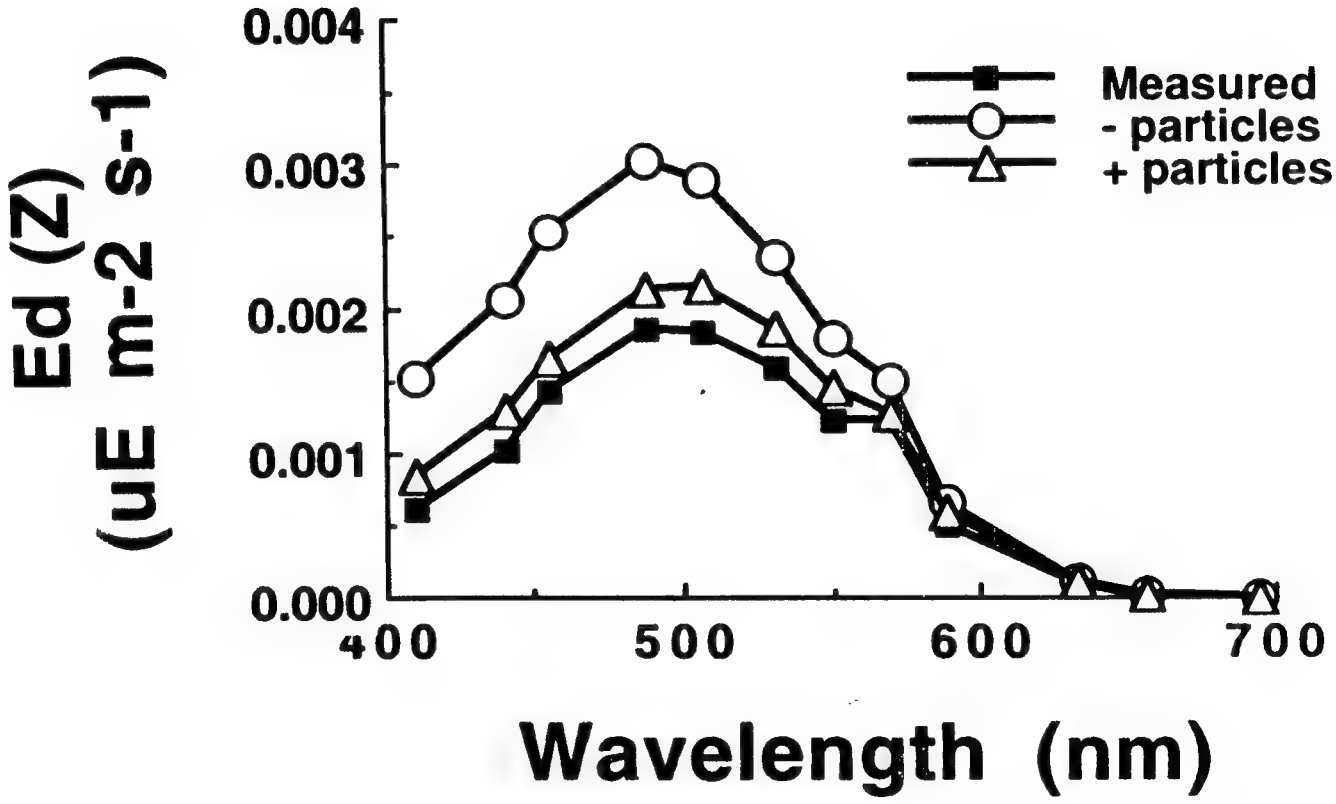

Fig C A
8.g84

Particle's effect on transmitted irradiances (FIRST YEAR ICE)

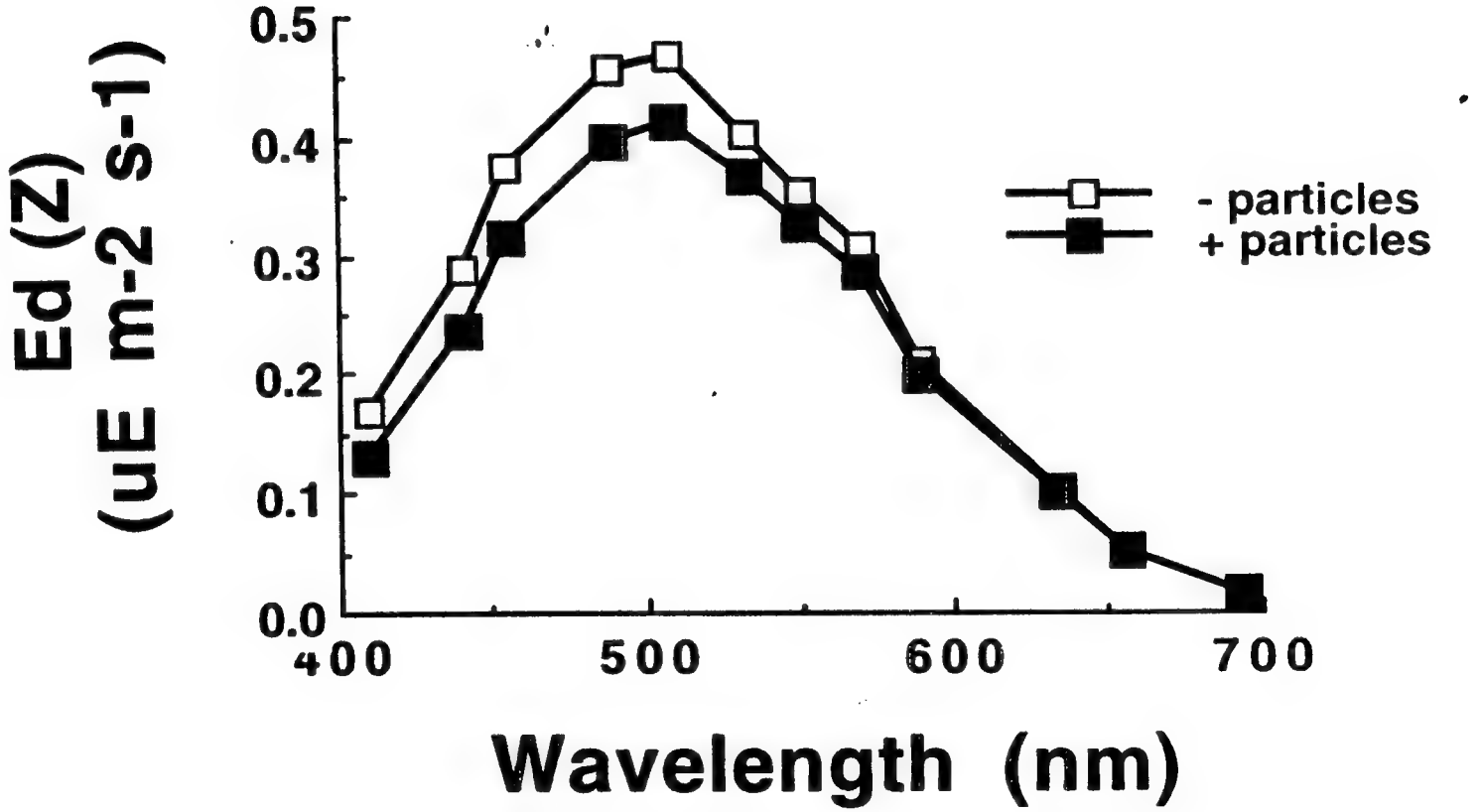

Fig 6 B

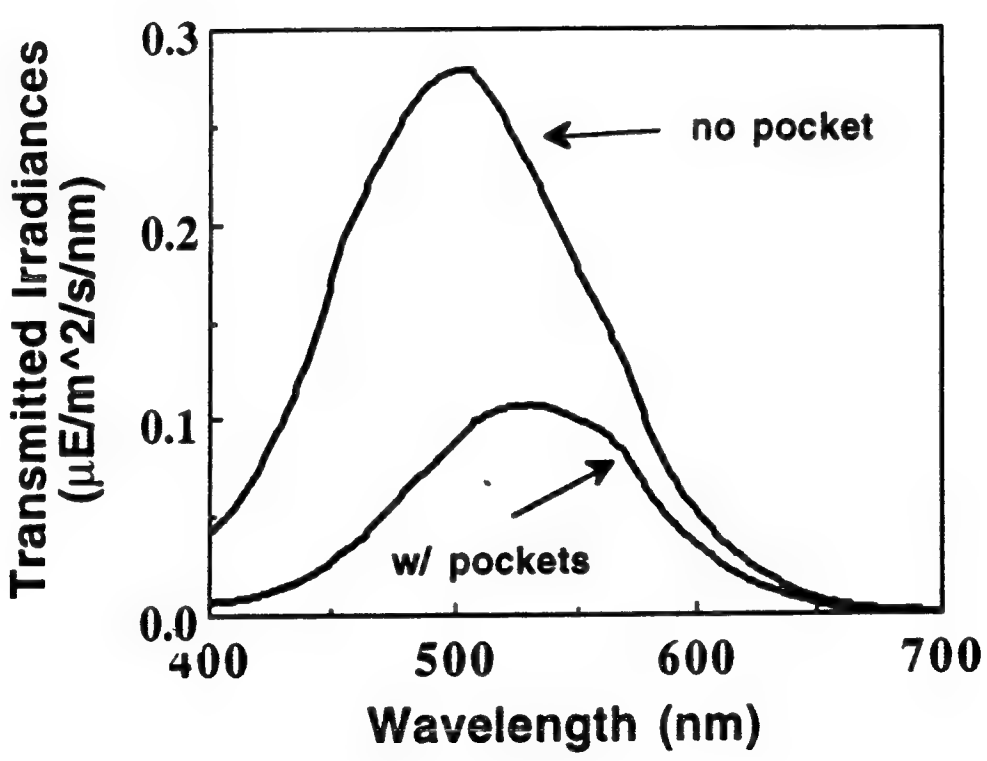
Transmitted Irradiances
(μE/m^2/s/nm)
0.3
0.2
0.1
0.0
400
500
600
700
Wavelength (nm)
no pocket
w/ pockets

Fig 6C

Algae's effect on transmitted irradiances beneath FIRST YEAR ice

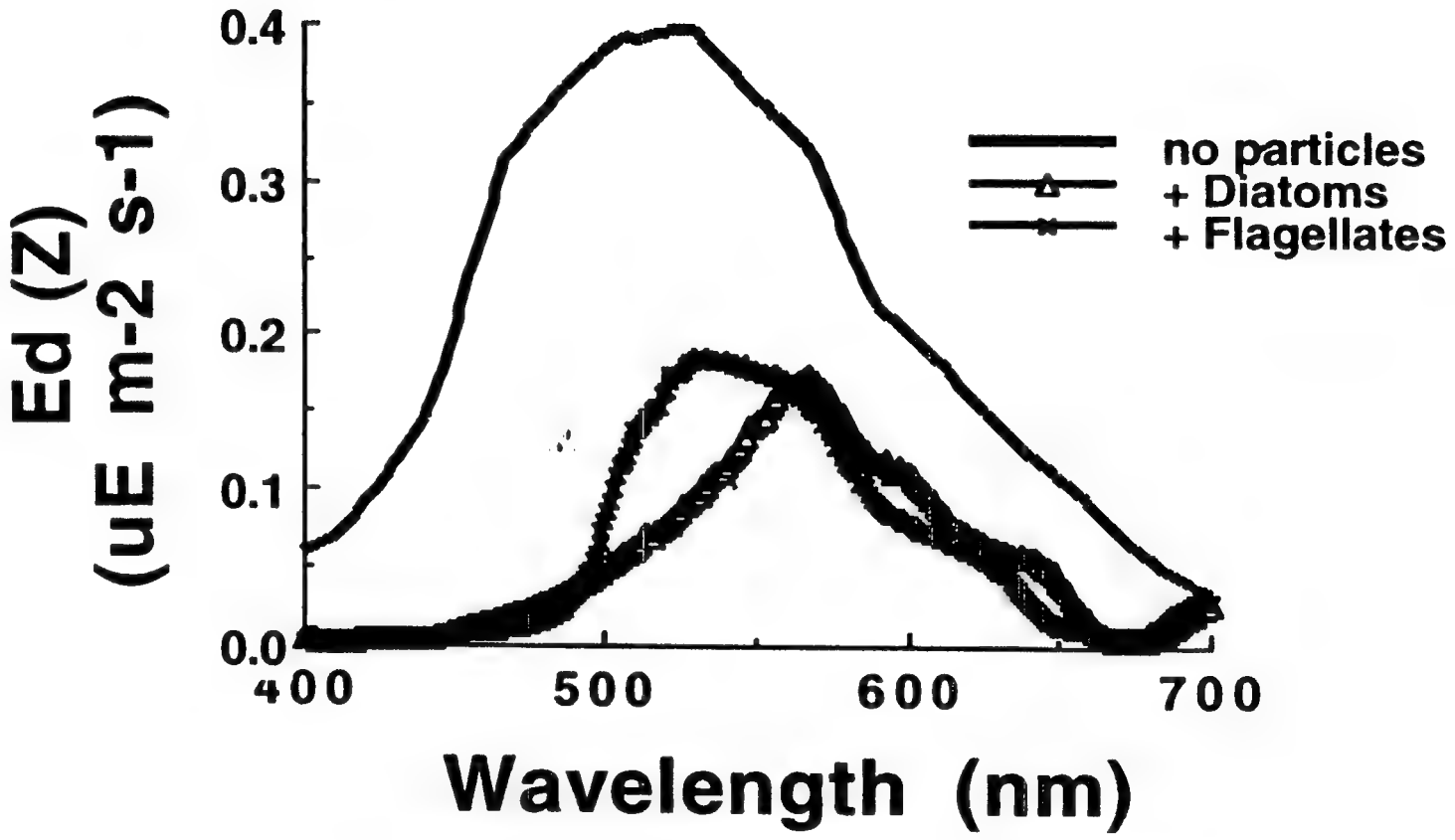

Fig 7B.

The effect of particle type on transmitted irradiances

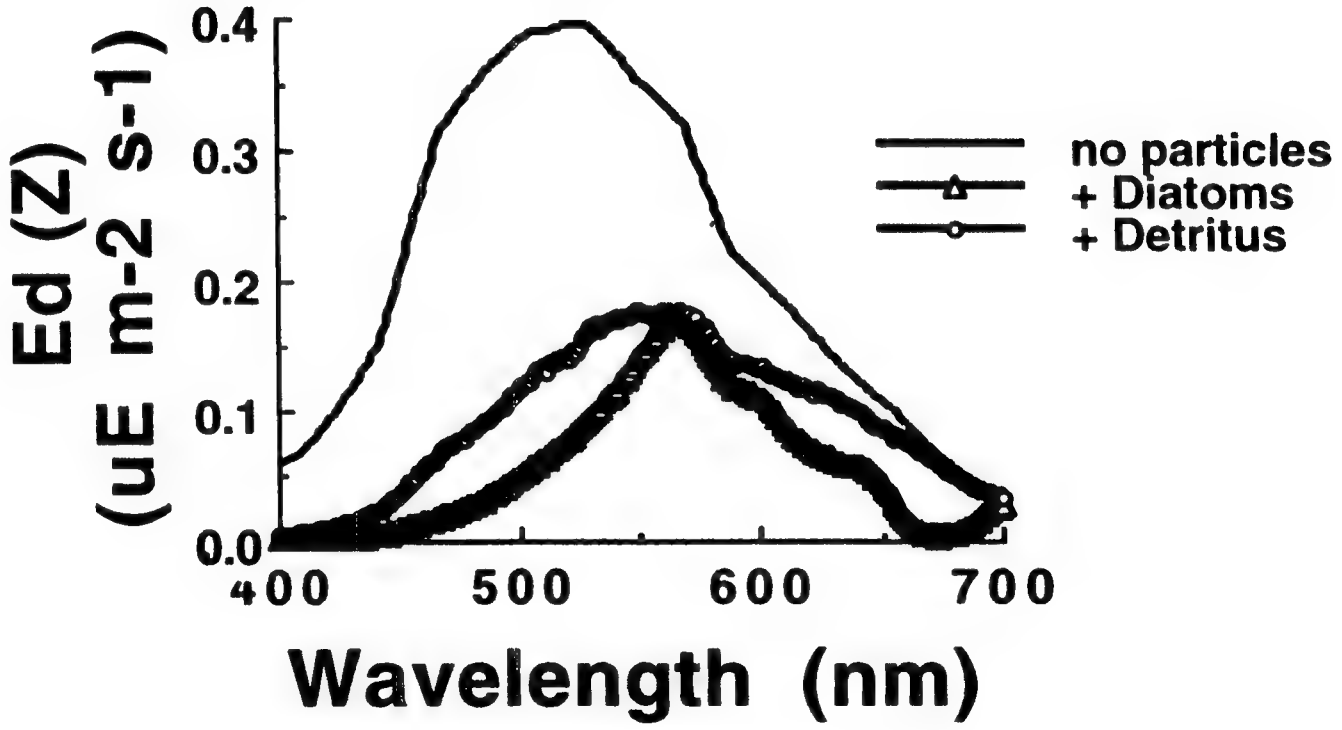

Fig 7A

References:

Arrigo, K. R., C. W. Sullivan, and J. N. Kremer. 1992. A bio-optical model of Antarctica sea ice. J. Geophys. Res. 96(c6): 10,581-10592.

Bidigare, R.R., M.E. Ondrusek, J.H. Morrow, and D.A. Kiefer, 1988. *In vivo* absorption prpoerties of algal pigments. SPIE vol. XXXX Ocean Optics X:1302-1321.

Bricaud, A. and D. Stramski. 1990. "Spectral absorption coefficients of living phytoplankton and nonalgal biogenous matter: A comparison between the Peru upwelling area and Sargasso Sea," Limnol. Oceanogr., 35(3): 562-582.

Butler, W.L., 1962. Absorption of light by turbid materials. J. Opt. Soc. Am. 52:292-299.

Buynitsky, V.K., 1968. The influence of microalgae on the structure and strength of Antarctic sea ice. Oceanology 8:771-767.

Clark, A.D., and K.J. Noone. 1985. Soot in the Arctic snow pack: a cause for perturbations in radiative transfer. Atmospheric Environment. 19(12):2045-2053.

Fritsen, C.F., R. Iturriaga, and C.W. Sullivan., 1992. Influence of particulate matter on spectral irradiance fields and energy transfer in the Eastern Arctic Ocean. SPIE vol. 1750 Ocean Optics XI:527-541.

Grenfell, T. C. and G. A. Maykut, 1977. The optical properties of ice in the Arctic Basin, J. Glaciol., 18: 445-463.

Grenfell, T.C., 1991. A radiative transfer model for sea ice with vertical structure variations. J. Geophys. Res., 96(C9): 16,991-17,001.

Grenfell, T.C., 1983. A theoretical model of the optical properties of sea ice in the visible and near infrared. J. Geophys. Res. 88(C14):9723-9735.

Grossi, S.M., S.T. Kottmeier, R.L. Moe, G.T. Taylor, and C.W. Sullivan, 1987. Sea ice microbial communities. V. Growth and primary production in bottom ice under graded snow cover," Mar. Ecol. Prog. Ser., 35: 153-164.

Iturriaga, R., and D.A. Siegel, 1988. Discrimination of the absorption properties of marine particulates using a

microphotometric technique," SPIE vol. 925 Ocean Optics IX, 277-287.

Iturriaga, R., and D.A. Siegel, 1989. Microphotometric characterization of phytoplankton and detrital absorption in the Sargasso Sea. Limnol. Oceanogr., 34: 1706-1726.

Kishino, M., C.R. Booth, and N. Okami, 1984. Underwater radiant energy absorbed by phytoplankton, detritus, dissolved organic matter, and pure water. Limnol. Oceanogr., 29: 340-349.

Larssen, B. B., A. Elverhoi and P. AAgaard, 1987. Study of particulate material in sea ice in the Fram Strait -a contribution to paleoclimatic research? Polar Res., 5(3): 313-315.

Legendre, L., and M. Gosselin, 1991. In situ spectroradiometric estimation of microalgal biomass in first-year sea ice. Polar biol. 11: 113-115.

Lewis, M.R., J.J. Cullen, and T. Platt, 1983. Thermal structure in the upper ocean: Consequences of nonuniformity in chlorophyll profile, J. Geophys. Res., 88, 2565-2570.

Lewis and Cota, unpublished, Radiation absorption by ice algae: influences on the heat budget of Arctic sea ice.

Maykut,G.A., and T.C. Grenfell, 1975. The spectral distribution of light beneath first-year sea ice in the Arctic Ocean," Limnol. and Ocean., 20: 554-563.

Maykut, G.A., 1986. The surface heat and mass balance. pp 395-464 In: The Geophysics of Sea Ice. N. Untersteiner, ed. Plenum Press, NY.

Maykut, G.A., and D.K. Perovich, 1987, the role of shortwave radiation in the summer decay of a sea ice cover. J.Geophys. Res. 92(C7):7032-7044.

Mitchell, B.G., and D.A. Kiefer, 1987. Determination of absorption and fluorescence excitation spectra for light limited phytoplankton. in Marine phytoplankton and productivity, O. Holm-Hansen et al.(eds), pp. 157-169. Springer.

Morel, A., and A. Bricaud, 1981. Theoretical results concerning light absorption in a discrete medium, and application to specific absorption of phytoplankton. Deep-Sea Res., 28A: 1375-1393.

Palmisano, A.C., J.B. SooHoo, R.L. Moe, and C.W. Sullivan, 1987. Sea ice microbial communities. VII. Changes in under-ice spectral irradiance during the development of Antarctic sea ice microalgal communities. Mar. Ecol. Prog. Ser., 35: 165-173.

Perovich, D.K., 1990.Theoretical estimates of light reflection and transmission by spatially complex and temporally varying sea ice covers," J. Geophys. Res., 95(C6): 9557-956 .

Perovich, D.K., G.F. Cota, G.A. Maykut, and T.C. Grenfell, 1993, Bio-optical observations of first-year Arctic sea ice. Geophysical Res. Letts. 20(11):1059-1062.

Pfirman,S., J.C. Gascard, I. Wollenburg and A. Abelmann, 1989. Particle-laden Eurasian Arctic sea ice: observations from July and August 1987. Polar Res, 7(1): 313-315.

Platt, T., M.R. Lewis, and R. Geider. 1983. thermodynamics of the pelagic ecosystem: Elementary closure conditions for biological production in the open ocean. in Flows of Energy and Materials in the Marine Environment. ed. M. Fasham, Plenum, New York.

Reiminetz, E., P.W. Barnes, W.S. Weber, 1993. Particulate matter in pack ice of the Beufort Gyre. J. Glaciol. 39(131): 186-197.

Roesler. C.S., M.J. Perry, and K.L. Carder. 1989. Modeling in situ phytoplankton absorption from total absorption spectra in productive inland waters. Limnol. Oceanogr. 34(8)1510-1523.

Truper, H.G. and C.S. Yentsch, 1967. Use of glass fiber filters for the rapid preparation of in vivo absorption spectra of photosynthetic bacteria. J. Bact. 94:1255-1256.

Wiscombe, W. J., and S. G. Warren. 1982. A Model for the spectral albedo of snow. I: Pure snow. J. Atmos. Sci. 37: 2712-2733.

Office of Naval Research
U.S. Navy
Proudly Presents

Best Student Paper Award
Ocean Optics XI

Awarded to

Chris H. Fritsen

For significant and original research, attention to quality, and professionalism in the oral and written presentation.

22 July 1992
San Diego, California

Attested by

Gary D. Gilbert, Office of Naval Research
Curtis D. Mobley, NASA Jet Propulsion Lab.
Richard W. Spinrad, Office of Naval Research
Joan S. Cleveland, San Diego State Univ.
Jules S. Jaffe, Scripps Institution of Oceanography
Donald K. Perovich, U.S. Army Cold Regions Research and Engineering Lab.
and
Theodore T. Saito, 1992 President of
SPIE—The International Society for Optical Engineering

Best Student Paper Award
Ocean Optics XI

20-22 July 1992
San Diego, California

The Office of Naval Research (ONR) of the U.S. Navy, in conjunction with SPIE—The International Society for Optical Engineering, is proud to award this honorarium and certificate for the best student paper presented at the Ocean Optics XI Conference held in San Diego, California, as part of the 1992 SPIE Symposium on Optical Applied Science and Engineering. This award is presented in recognition of superlative research and outstanding formal presentation by the recipient. The award recognizes the high standards of achievement supported by ONR and SPIE in the fields of hydrologic optics and optical oceanography.

It is with great pleasure that we present this Best Student Paper Award and offer our best wishes for a long and influential career in the area of ocean optics.

Gary D. Gilbert
Office of Naval Research

Theodore T. Saito
President
SPIE—The International Society
of Optical Engineering

Influence of particulate matter on spectral irradiance fields and energy transfer in the Eastern Arctic Ocean.

Chris H. Fritsen

Rodolfo Iturriaga

University of Southern California
Department of Biological Sciences
Los Angeles, CA 90089-0371

Cornelius W. Sullivan

University of Southern California,
Graduate Program in Ocean Sciences
Hancock Institute for Marine Studies
Los Angeles, CA 90089-0373

ABSTRACT

Time series studies of the spectral irradiance fields beneath multiyear pack ice were conducted in the Eastern Arctic Basin at 82-83°N as part of the Coordinated Eastern Arctic Research Experiment (CEAREX). Particulate matter was collected from the multiyear pack ice as well as first year ice in a refrozen lead. The vertical distribution within the ice and the spectral absorbtion properties of the particulates were determined in order to estimate their contribution to the optical properties of the sea ice.

Among the particulates contained in sea ice detritus was common throughout all portions of the pack ice and was the major light absorbing particulate matter in the ice at the time of the observation. Algal cells and mineral-like particulates also were present, yet they contributed to the light-absorbing properties to a lesser extent than the detritus. During early spring, particulate matter contributed little to the bulk attenuation coefficients of the multiyear ice, however, it was estimated to have a more substantial contribution to the attenuation coefficients of first year ice in a refrozen lead. Results of a single stream multilayer radiative transfer model that simulates concentrations of biogenic particulate matter observed in Arctic sea ice indicates that particulate matter within sea ice plays a substantial role in radiative energy transfer and has the potential to seasonally alter spectral irradiance regimes within the ice covered Arctic ocean.

1. Introduction

In the ice covered regions of the polar oceans, the transfer of electromagnetic radiation (EMR) into the upper layers of the water column is strongly dependent on the inherent optical properties of the sea ice and snow. Particles, which are sometimes referred to as contaminants[1,2] will contribute to the inherent optical properties of the ice cover to varying degrees depending on their concentrations and their absorption and scattering properties. The influence of particles on the transmission of irradiance through sea ice has been observed in the field by many workers.[3,4,5,6]

Recently, two modeling efforts have incorporated the effects which particulate matter has on the propagation of EMR in sea ice. Arrigo et al[7] developed and then tested with field data a bio-optical model describing seasonal changes in downwelling spectral irradiances (400-700 nm) within and beneath land-fast congelation/platelet ice containing biogenic particles. Grenfell[8] included absorption and scattering terms for impurities in a two-stream multi-layer radiative transfer model for sea ice. These models indicate that absorption properties of different species, taxonomic groups, or assemblages of microalgae may cause substantial variability in the quantity and quality of under-ice spectral irradiances within the visible spectrum (400-700 nm).

During the 1989 Coordinated Eastern Arctic Experiment (CEAREX) we collected particulate matter from the sea ice North of Svalbard Norway during the early spring. The relative abundance and morphology of particle types and their light absorbing properties were determined. A concurrent assessment was made of the ambient surface and under-ice spectral irradiance fields in order to estimate the influence of the particulate matter on the apparent optical properties of the

sea ice. Single stream multilayer radiative transfer models are utilized to estimate the influence these particles play in energy transfer and alterations of spectral irradiance fields.

2. METHODS

2.1. Irradiance measurements

During operations at the CEAREX oceanographic camp (designated "O" camp) (originally located at 82°N, 10°W) irradiance measurements were made from April 7 to April 22. Measurements included: under-ice spectral downwelling irradiance ($E_d(z,\lambda)$), surface downwelling spectral irradiance ($E_d(0+,\lambda)$, and surface downwelling scalar irradiance ($E_{od}(0+,PAR)$) as photosynthetically available radiation (PAR) (400-700nm). $E_{od}(0+,PAR)$ was measured with a Biospherical Instruments model QSR-200 Solar Reference Hemispherical Irradiance sensor. Spectral measurements were made with a MER1010 spectroradiometer (Biospherical Instruments) with its 5 nm spectral band widths centered at 410, 441 455, 488, 507, 532, 550, 570, 589, 633, 656, and 694 nm. Both instruments were calibrated before and following the CEAREX 89 experiments at Biospherical Instrument company in San Diego, California.

Under-ice measurements with the undisturbed snow cover intact were made by mooring the spectroradiometer on an articulated arm deployed through a 75 cm diameter hydrohole (HH) drilled with a steam heat drill. The instrument was positioned at the ice/water interface approximately 3 m away from the hole which was covered to avoid stray light from reaching the cosine collector. With the radiometer still in position, natural snow cover was manually removed from above the radiometer in order to estimate the bulk diffuse spectral attenuation coefficients for the sea ice and snow using methods described below.

2.2. Sample collections

Two study sites were established where under-ice irradiances were measured and ice cores were also obtained. These will be referred to as HH1 and HH2. HH1 and HH2 were located in a relatively flat area among hummocked ice. Ice thickness was 2.75 meters and snow cover was 20 to 30 cm. Average salinities were 3-4 ppt (data not shown). Ice thickness, surface topography, snow cover, and low salinities indicate this was multiyear ice. An additional study site was established in an undeformed refrozen lead (L) with 1.2 meter thick ice having 10 to 20 cm snow cover. Two ice cores, designated L1 and L2 were obtained from this site with average salinities of 5-6ppt. The relatively high salinities, lack of deformation, and ice and snow thickness indicate that this was ice which had formed in the previous winter (i.e. first year ice).

Ice cores were obtained using a CRREL auger (7 cm diameter), sectioned, and then allowed to melt at 2°C in closed opaque containers. Samples for the analysis of the absorption properties of the particulate material were obtained from this meltwater and were analyzed according to methods described below.

2.3. Diffuse Attenuation Coefficient for Snow, $K_{dsnw}(\lambda)$

When the snow cover was removed from above the radiometer, the diffuse spectral attenuation coefficient for the natural snow cover $K_{dsnw}(\lambda)$ (m^{-1}) was estimated using the Beer-Lambert model describing the exponential attenuation of light through a homogenous medium.

$$K_{dsnw}(\lambda) = -\frac{1}{H} * \ln \frac{E_d(+snw,\lambda)}{E_d(-snw,\lambda)} \qquad (1)$$

where H is the thickness of the snow in meters and $E_d(+snw,\lambda)$ and $E_d(-snw,\lambda)$ are the under-ice downwelling spectral irradiances ($\mu E\ m^{-2}\ s^{-1}$) with and without snow, respectively.

2.4. Diffuse attenuation coefficient for sea ice, $K_{dice}(\lambda)$

Also using the Beer-Lambert model, the bulk diffuse spectral attenuation coefficient for optically thick sea ice ($K_{dice}(\lambda)$) can be approximated from the following relationship:

$$K_{dice}(\lambda) = -\frac{1}{z} * \ln \frac{E_d(z,\lambda)}{E_d(0-,\lambda)} \quad (2)$$

(9,10) where z is the thickness of the ice in meters, $E_d(z,\lambda)$ is the downwelling irradiance at the bottom of the ice and $E_d(0-,\lambda)$ is the downwelling irradiance just below the surface of the ice. $E_d(0-,\lambda)$ cannot be measured directly in the field but can be estimated as

$$E_d(0-,\lambda) = E_d(0+,\lambda) * (1- R_o) \quad (3)$$

where R_o is the specular reflection from the sea ice surface which is estimated according to Arrigo et al.[7]

2.5. Attenuation coefficient of particulate matter, $K_{dp}(\lambda)$

Attenuation of downwelling irradiance in a medium is due to the combined attenuation due to the medium itself and attenuation by particles and dissolved substances within the medium.[11,12] Ignoring attenuation by dissolved substances, the diffuse spectral attenuation coefficient for sea ice may be approximated by:

$$K_{dice}(\lambda) = K_{di}(\lambda) + K_{dp}(\lambda) \quad (4)$$

where $K_{dp}(\lambda)$ is the spectral diffuse downwelling attenuation coefficient of particulate material and $K_{di}(\lambda)$ is the spectral diffuse downwelling attenutation coefficient of pure sea ice. Furthermore, $K_{dp}(\lambda)$ can be approximated by

$$K_{dp}(\lambda) = \frac{a_p(\lambda) + b_p(\lambda)}{u_d(z)} \quad (5)$$

(13) where $a_p(\lambda)$is the total particulate absorption coefficient (m^{-1}), $b_p(\lambda)$ is the particulate backscattering coefficient (m^{-1}) and $u_d(z)$ is the mean cosine of the angular distribution of downwelling irradiance which is assumed to be 0.656.[14] Backscattering by sea ice particulate matter was not measured and will not be taken into account at the present time in order to approximate $K_{dp}(\lambda)$.

2.6. Particulate Absorption Coefficient, $a_p(\lambda)$

In order to estimate spectral light absorbing properties of the particulate matter contained within the ice, ice core meltwater was filtered through glass fiber filters (GF/f) and the spectral absorption coefficient of the total particulate matter ($a_p(\lambda)$) was estimated utilizing filter pad methods which have been described previously.[5,15,16]

2.7. Absorption Efficiency of Individual Particles, $Q_a(\lambda)$

In order to determine the light absorbing properties of individual particles, ice core meltwater was filtered through 0.4 µm pore size Nuclepore filters at low pressures (5 mmHg). Particles retained by the filters were immediately transferred to gelatin coated microscope slides[17] and kept frozen until they were analyzed at USC. Absorption efficiency spectra of the individual particles were determined using a microphotometric technique.[18]

2.8 Particule's contribution to $K_{dice}(\lambda)$)

A vertically averaged absorption coefficient $\langle a_p(\lambda)\rangle$ of the sea ice particulate matter can be calculated as,

$$\langle a_p(\lambda)\rangle = \frac{\Sigma a_p(\lambda)_n * Z_n}{Z} \quad (6)$$

where $a_p(\lambda)_n$ (m^{-1}) is the particulate absorption and Z_n (m) is the thickness of each section (n) of the ice core. By substituting $\langle a_p(\lambda)\rangle$ for $a_p(\lambda)$ in equation 10 a vertically averaged particulate attenuation coefficient $\langle K_{dp}(\lambda)\rangle$ for the ice cover can be approximated. $\langle K_{dp}(\lambda)\rangle$ estimated in this manner represents a weighted average over the entire ice thickness

and, therefore, does not rely on or account for vertical variations in particulate concentrations. $<K_{dp}(\lambda)>$ can then be used to approximate the particulate matter's contribution to the sea ice attenuation coefficients, $F(\lambda)$,by

$$F(\lambda) = \frac{<K_{dp}(\lambda)>}{K_{dice}(\lambda)}. \quad (7)$$

2.9. Modeling energy absorption within sea ice

EMR absorption by the constituents of a homogeneous medium depends on the constituent's absorbing properties, their vertical distribution, and the irradiance distribution within the medium. Given the absorption coefficient of constituent x, the attenuation coefficient ($K_d(\lambda)$) for the medium and assuming a homogenous distribution of each constituent within the medium, the rate of EMR absorption by constituent x ($E^x_{abs}(\lambda)$) can be approximated by

$$E^x_{abs}(\lambda) = [E_d(0\text{-},\lambda) - E_d(Z,\lambda)] * \frac{a_x(\lambda)}{K_d(\lambda)} \quad (8)$$

where $E_d(0\text{-},\lambda)$ is the downwelling irradiance just below the surface of the medium, $E_d(Z,\lambda)$ is the transmitted downwelling spectral irradiance. The ratio of the absorption coefficient to the attenuation coefficient simply is the fraction of attenuated downwelling irradiances lost to absorption by constituent x. $E_d(Z,\lambda)$ can be determined according to the Beer-Lambert model.

$$E_d(Z,\lambda) = E_d(0\text{-},\lambda) * e^{(-K_d(\lambda) * Z)}. \quad (9)$$

$E^x_{abs}(\lambda)$ can be spectrally integrated using a finite integration scheme

$$E^x_{abs} = \int_{\lambda=400}^{700} E^x_{abs}(\lambda)\, d\lambda \quad (10)$$

in order to obtain the rate of absorption of total visible EMR by each constituent within the medium. Because sea ice usually consists of multiple layers with distinct optical properties equations 8,9, and 10 are applied for multiple layers when modeling absorption within a sheet of sea ice. At the surface of the ice or snow, specular reflection is modeled according to Arrigo et al[7] and specular reflection at the interface between layers is assumed to be zero.[1,7] For our purposes, x is considered to be either pure sea ice (i) or particulate material (p). We wished to model the partitioning of visible EMR that was absorbed by the sea ice and particulates within the ice, and the EMR passing into the water column. This was accomplished by combining equations 3,4, 8, and 9 and specifying an incident spectral irradiance (400-700 nm) (figure 2), attenuation coefficients for snow (figure 1b), absorption coefficients for the sea ice as "bubble free" sea ice,[19] attenuation coefficients of sea ice,[1,3,7] and absorption coefficients for the particulates within the ice.

3. RESULTS

3.1. Diffuse Attenuation Coefficient for Snow, $K_{dsnw}(\lambda)$

Under-ice spectral downwelling irradiances on Julian day 97 and 98 (April 7 and 8) with and without the natural snow cover intact are shown in figure 1a. Using these measurements, $K_{dsnw}(\lambda)$ was estimated according to equation #1 (figure 1b). The shape of the resultant $K_{dsnw}(\lambda)$ spectrum is typical for snow[1], however, the magnitude is low compared to dry compact snow[20] but may be reasonable for an ice-snow mixture which was observed at this site. The low values may also be an artifact because specular reflection from the air/ice interface is not taken into account in equation #1.

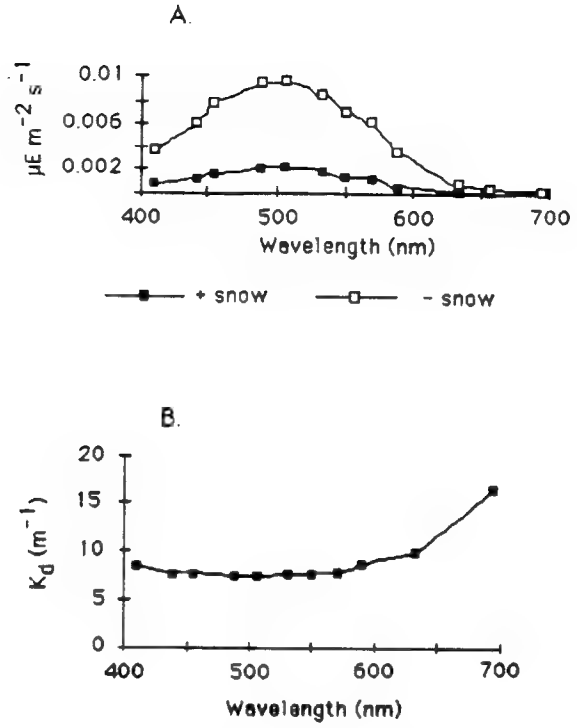

Figure 1. A) Downwelling spectral irradiances beneath 2.4 meters of multiyear ice with and without 20 centimeters of snow. $E_{od}(0+,PAR)$ = 1721 and 1711 $\mu E\ m^{-2}\ s^{-1}$ during the measurement periods with snow and without snow, respectively. B) Estimated diffuse attenuation coefficient of the snow cover based on spectra shown in A.

3.2. Diffuse attenuation coefficients for sea ice, $K_{dice}(\lambda)$

Diel time series of surface downwelling spectral irradiances on JD 99 under clear skies are shown in figure 2a. When normalized to their peak wavelengths (figure 2b) it is apparent that spectral shifting towards the shorter wavelengths occured at increased solar angles. This is consistent with a shifting toward a more diffuse skylight which is predominantly blue.[21] Under-ice downwelling spectral irradiances at the HH1 position are shown in figure 3 with the snow cover removed and the sky state was similar to that of JD 98 when measurements of the surface downwelling spectral irradiances were made. Note that spectral shifting towards the blue wavelengths also occurs beneath the ice (figure 3b).

$K_{dice}(\lambda)$ spectra for the HH1 and HH2 study sites are illustrated in figure 4. These values fall between those reported for a "white ice" granular or scattering layer or those for the interior portions of multi-year "white ice" or blue ice.[22] This is consistent with visual observations made in the field where it was noted that the top portions of 75 cm diameter ice cores were indeed white while the remainder of the cores appeared blue-green. Therefore, we recognize that the ice was not a structurally homogeneous medium but instead had at least two distinct layers that could be visually distinguished.

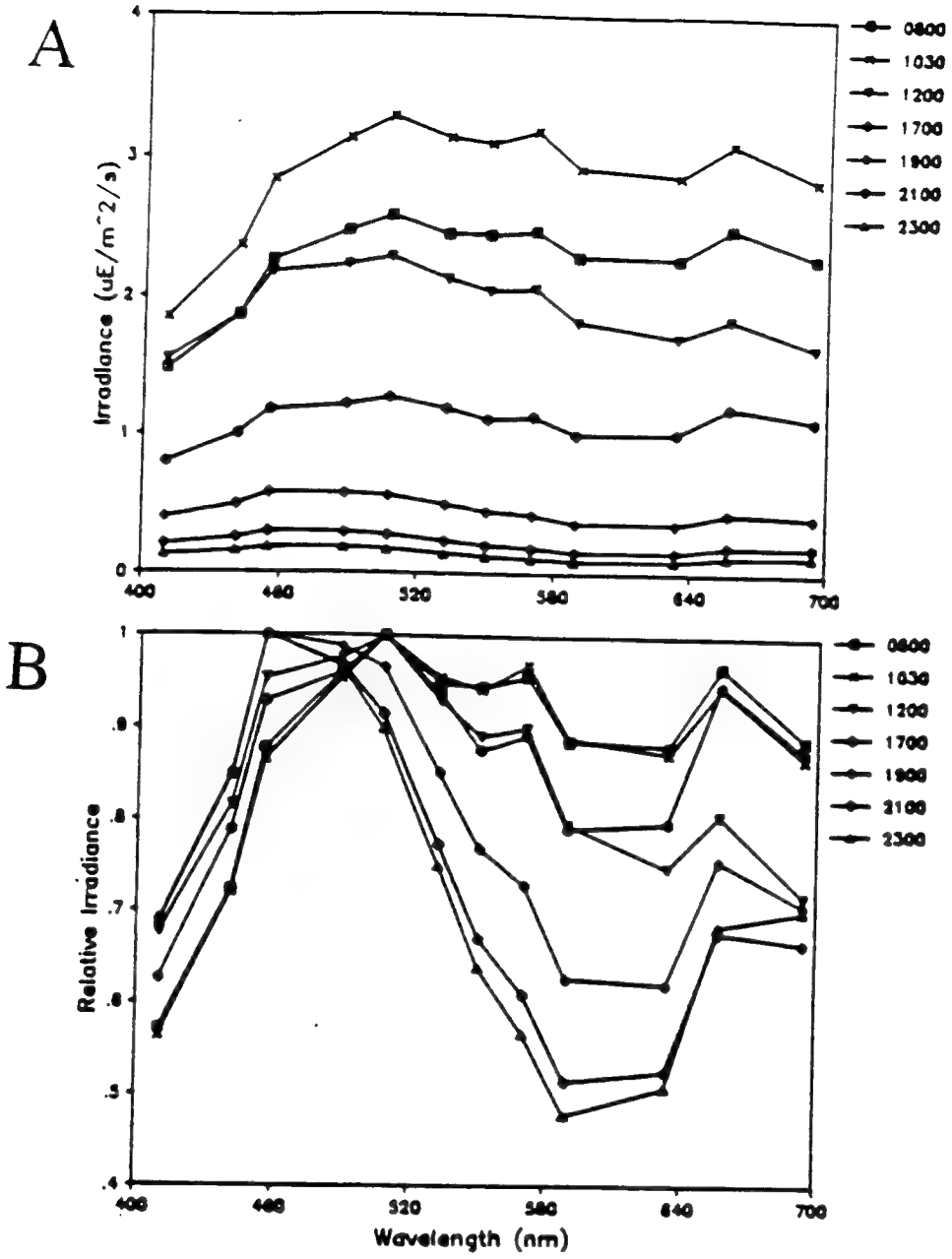

Figure 2. A) Diurnal time series of incident downwelling spectral irradiances measured between 0800 to 2300 hours on JD 99 B) Spectra were normalized to the peak wavelength in order to illustrate spectral shifting.

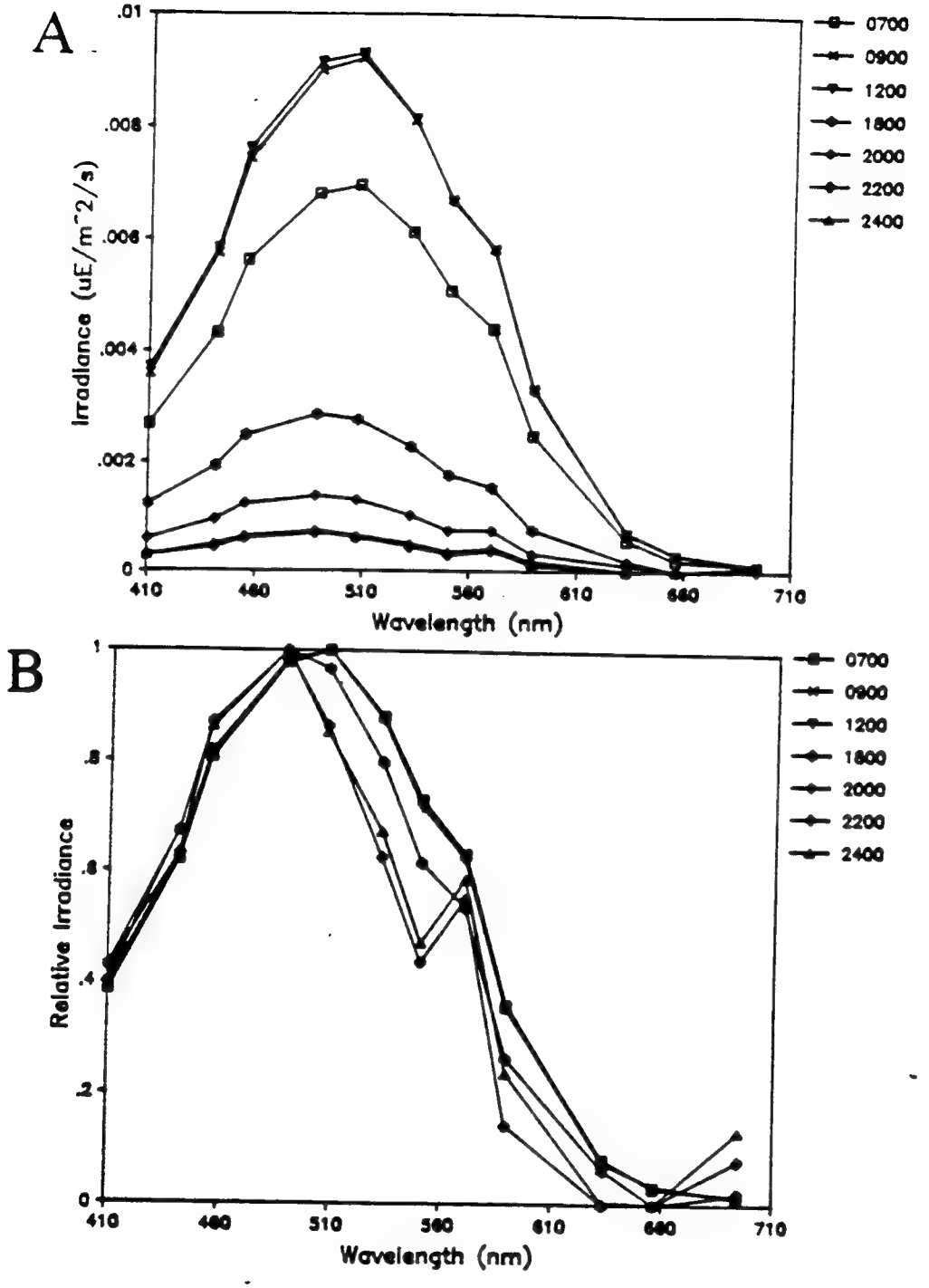

Figure 3. A) Diurnal time series of downwelling spectral irradiances beneath 2.75 meters of multiyear pack ice (HH1 sampling site) recored on Julian day 98. B) Spectra were normalized to the peak wavelength in order to illustrate spectral shifting.

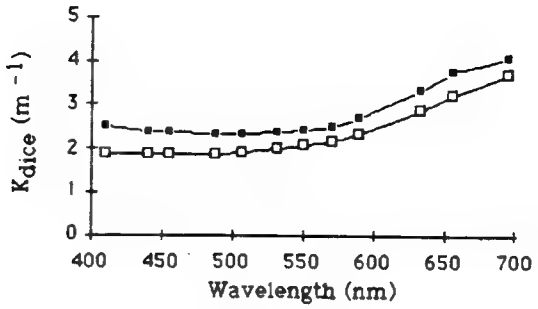

Figure 4. Spectral diffuse attenuation coefficients for the multiyear ice at HH1 (open squares) and the HH2 (solid squares) sites.

3.3. Individual particle's absorption efficiencies, $Q_a(\lambda)$

The ice cores from HH1 and HH2 contained faint bands of particulate matter, one meter below the ice/snow interface, visible to unaided eyes. Particulate matter was not visually apparent in the remaining sections of these cores nor in the cores from the refrozen lead. Microphotometric analysis revealed that **all** sections of the multiyear and lead ice cores contained a variety of fine grained (<500 μm) particulates. The multiyear ice contained a diverse assemblage of particulates including: empty diatom frustules, various species of pigmented pennate diatoms, tetrads of cells of unknown taxonomic affinity, arthropod remains, flocculant detrital material, individual mineral-like particulates, and aggregates containing all of the above mentioned material. The ice from the refrozen lead also contained particulates similar to that found in the HH1 and HH2 ice cores. Some of the microalgae found in the bottom sections, however, were morphologically distinct from those found in the HH1 and HH2 ice cores. Total pigment (chlorophyll a and pheopigment) concentrations were less than 0.15 mg m^{-3} in all sections of both the multiyear ice and ice from the refrozen lead.

$Q_a(\lambda)$ spectra of the microalgae found in the HH1 ice core are shown in figure 5. The majority of the cells (61%) were pennate diatoms ranging in size from 10 to 80 μm in length. Their $Q_a(\lambda)$ revealed shapes typical of spectra for marine diatoms having primary and secondary absorption peaks at 430 and 670 nm respectively.[23] There were, however, some pigmented cells with atypical absorption spectra. Most noteworthy were some pigmented spherical cells found in section A which were often found in tetrads. The cells were 8 to 20 μm in diameter and their absorption spectra were characterized by broad peaks centered around 470 to 480 nm. Furthermore, a few of the diatoms from the lower sections of the ice possessed very high absorption efficiencies with broad and flat primary and secondary absorption peaks indicative of packaged pigments or large cells.[23]

The non-algal particulates possesed $Q_a(\lambda)$ spectra with a wide variety of shapes (figure 5). The majority (70%) were amorphous aggregates of flocculant material with $Q_a(\lambda)$ being larger at shorter wavelengths and having a monotonic decrease towards the red wavelengths which is typical for detritus.[24] The remaining 30% of the non-algal particles appeared to be mineral-like particulates because of their characteristic angular edges, facets, and color. These also had high absorption efficiencies at shorter wavelengths. However, unlike the detritus, their $Q_a(\lambda)$ spectra were concave upward and were relatively high and flat from 400 to 525 nm with a rapid decline at the longer wavelengths. Mineral-like particulates ranged from 5 to 15 μm in diameter. Similar $Q_a(\lambda)$ spectra were measured from individual particulate matter from HH1 and HH2 ice cores.

3.4. Particulate matter absorption coefficients $a_p(\lambda)$

Absorption coefficients of the total particulate matter collected from the ice cores revealed that detritus was the predominant light absorbing particulates throughout vertical profiles of both ice types (figures 6,7,8,9). Section B of the HH1 ice core, was the only portion of this core which had $a_p(\lambda)$'s with a distinct chlorophyll absorption peak at 675 nm. All of the HH2 sections, on the other hand, had $a_p(\lambda)$'s with distinct absorption peaks at 675 nm. The $a_p(\lambda)$'s from the L1 and L2 ice cores showed the 675 nm absorption peak only in the bottom most sections of the cores. The HH2 ice core was

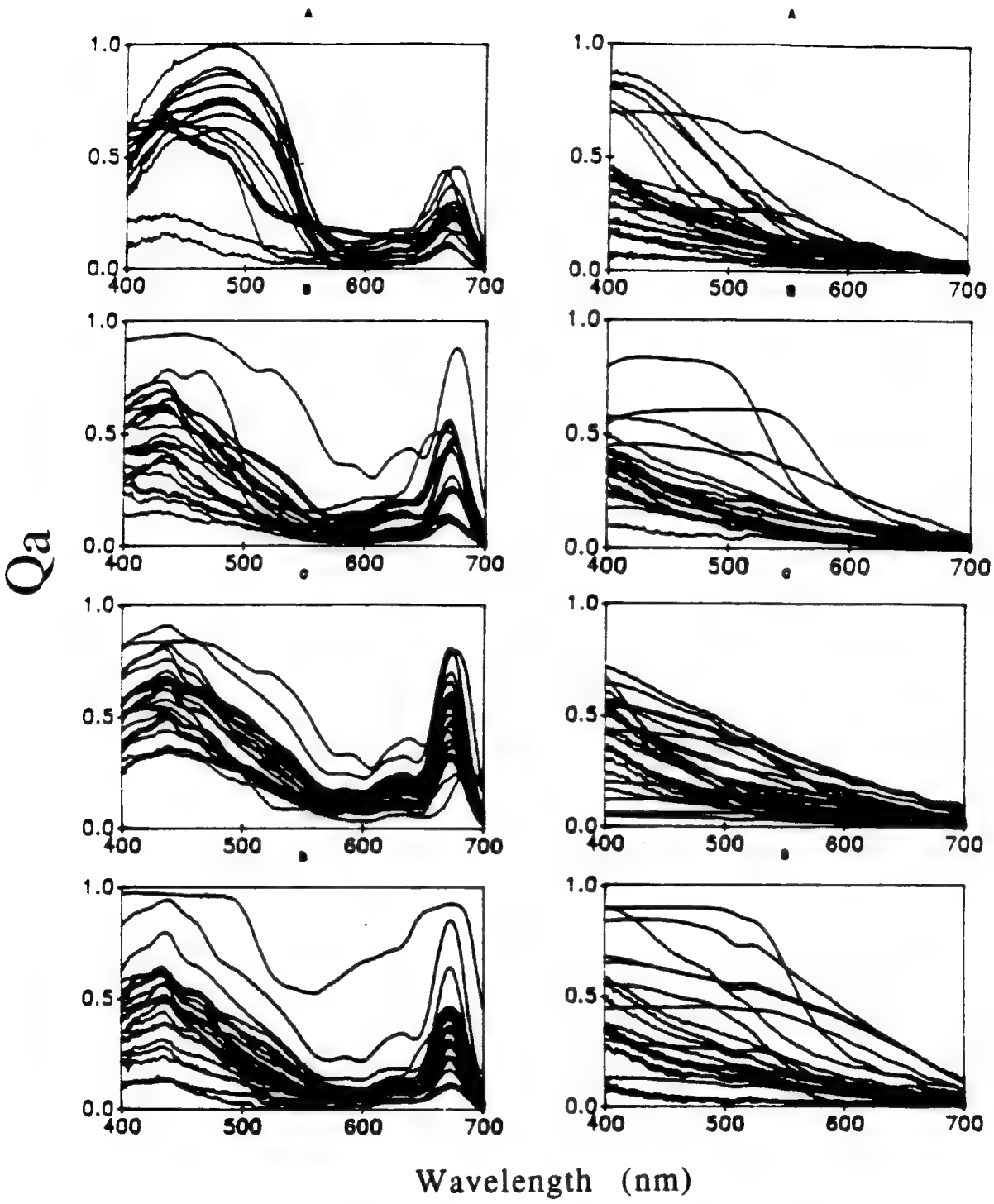

Figure 5. Absorption efficiency spectra of individual pigmented cells (left column) and non pigmented particles (right column) collected from discrete sections (A through D) of the multiyear ice core (HH1). Section locations within the HH1 ice core and thickness are illustrated in figure 6.

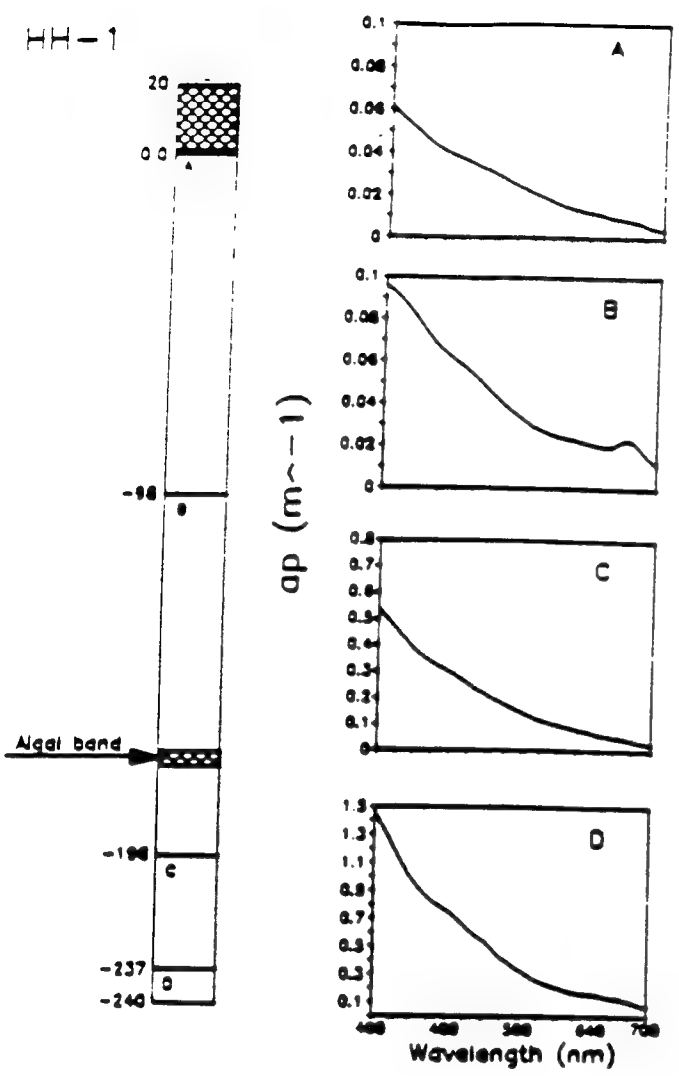

Figure 6. Diagram illustrating the multiyear ice core (HH1) and the particulate absorption coefficients as a function of wavelength (400-700nm) for the particulates collected from vertical sections A through D. A 5 cm thick algal layer is illustrated at 1.75 meters from the ice/snow intervace which was visually apparent in the field.

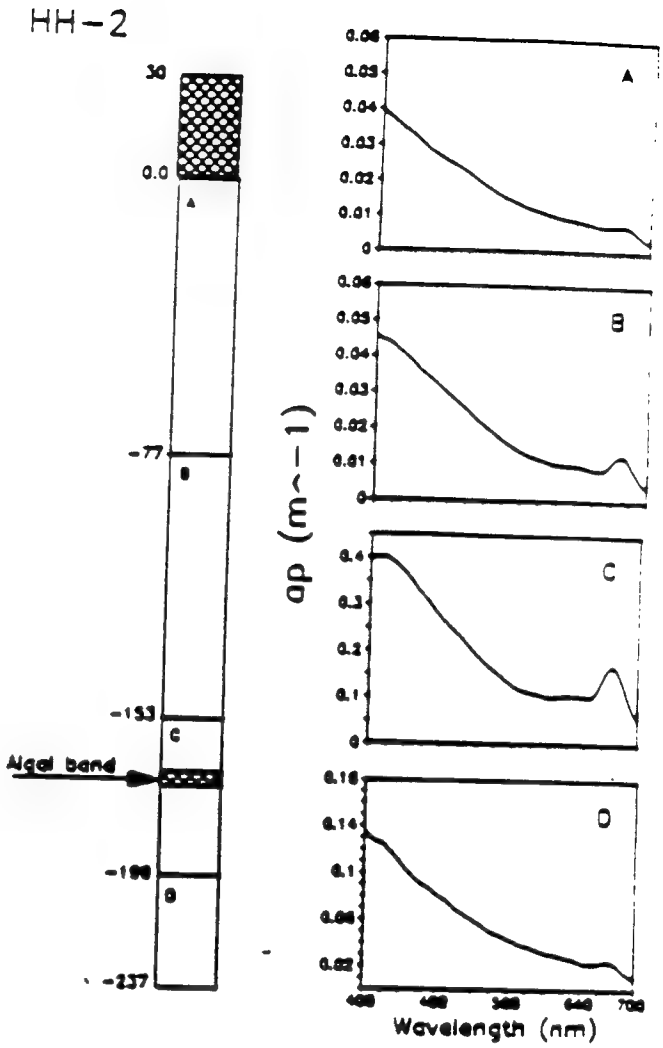

Figure 7 Diagram illustrating the multiyear ice core (HH2) and the particulate absorption coefficients as a function of wavelength (400-700nm) for the particulates collected from vertical sections A through D. A 5 cm thick algal layer is illustrated at 1.75 meters from the ice/snow intervace which was visually apparent in the field.

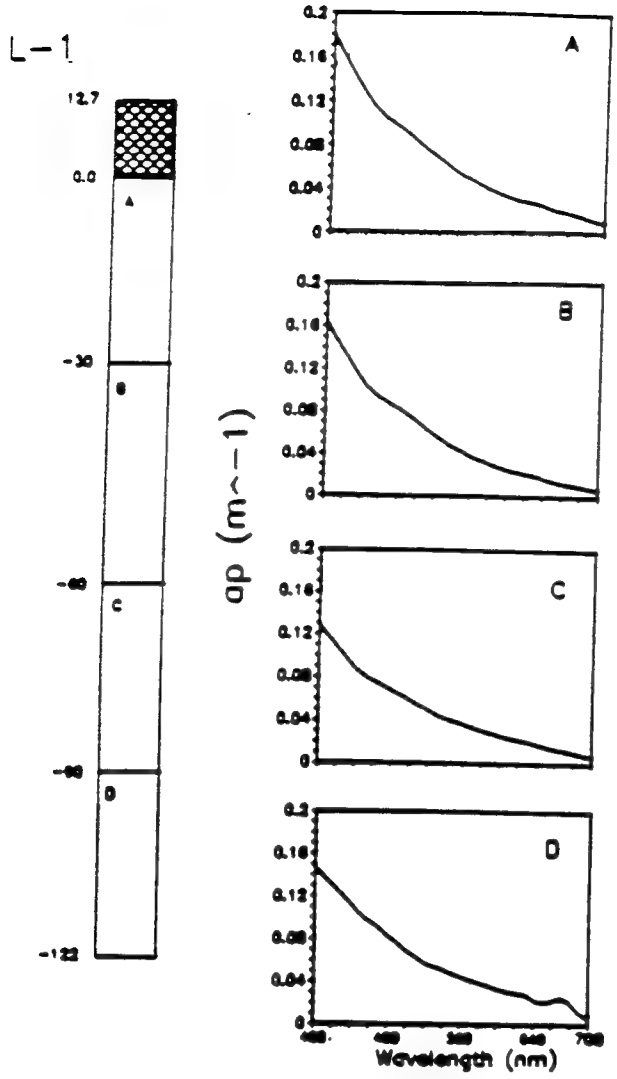

Figure 8 Diagram illustrating an ice core (L1) from a refrozen lead and the particulate absorption coefficients as a function of wavelength (400-700nm) for the particulates collected from vertical sections A through D of the core.

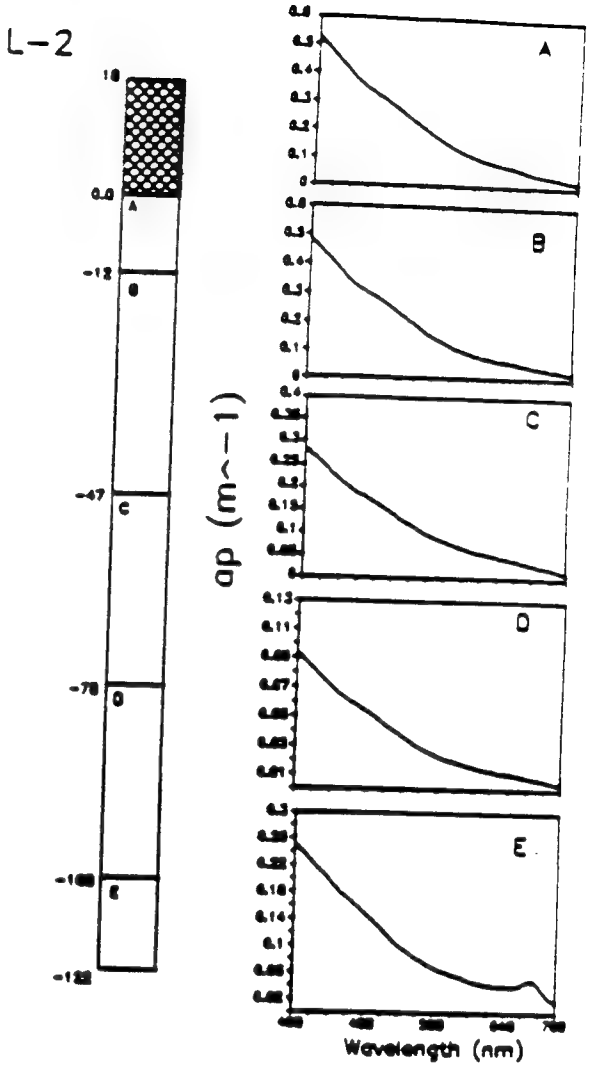

Figure 9 Diagram illustrating an ice core (L2) from a refrozen lead and the particulate absorption coefficients as a function of wavelength (400-700nm) for the particulates collected from vertical sections A through E of the core.

the only core containing particles with absorption peaks or shoulders in the 430-440 nm wavelengths indicative of living plant material. Despite these $a_p(\lambda)$'s showing characteristics of a microalgal component it is apparent that particulate absorption was dominated by the detritus. The $a_p(\lambda)$'s from an equivelent volume of the water column were 2 to 100 times lower than the $a_p(\lambda)$'s in the ice (data not shown), thus suggesting that particles are more concentrated in sea ice than in the water column.

3.5 Particles contribution to $K_{dice}(\lambda)$

Using the attenuation coefficients of multiyear ice (figure 4) and of blue first-year ice[1,22] as estimates of the attenuation coefficients of the multiyear ice and the lead ice, respectively, we estimated the ratio of the particulate attenuation coefficient to the total sea ice attenuation coefficient (figure 10). This ratio indicates that particulate material had their largest contribution at wavelenghts <500 nm where sea ice generally has low attenuation coefficients[1] and absorption by the particulate material is at its highest.

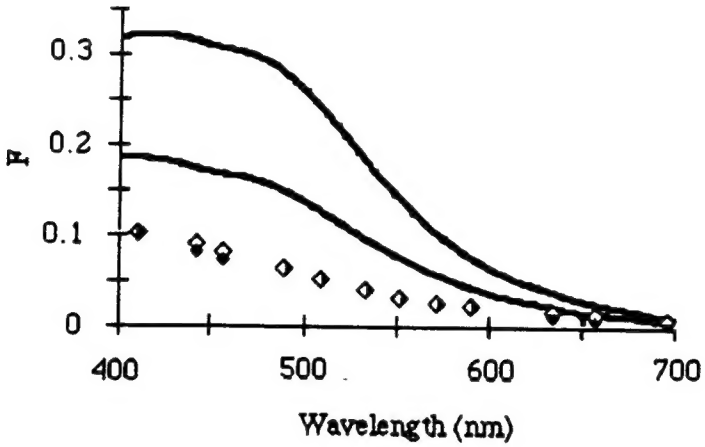

Figure 10. Estimates of the fraction of the sea ice attenuation coefficients due to particulate absorption (F) as a function of wavelength at four core sampling sites. Upper solid line = L2, lower solid line = L1, open diamonds = HH2, closed diamonds = HH1. F calculated according to equation 7. The attenuation coefficients for HH1 and HH2 are shown in figure 4 while attenuation coefficients of L1 and L2 were estimated by adding the attenuation coefficient of blue first-year ice[21] to the calculated $\langle K_{dp}(\lambda) \rangle$ for L1 an L2.

3.6 EMR absorption

The application of the energy absorption model indicates that particulate matter present at CEAREX "O" camp (i.e. L2) was the major energy absorbing constituent within the sea ice. The fraction of the energy being absorbed by the particles within the ice becomes more pronounced as snow depth increases (rows 1-4, table 1). This is caused by the snow shifting the transmitted irradiance towards wavelengths which are readily aborbed by particulate matter. The magnitude of energy absorption by both the sea ice and the particles is strongly reliant on snow depth which has been demonstrated previously. [1,2,3]

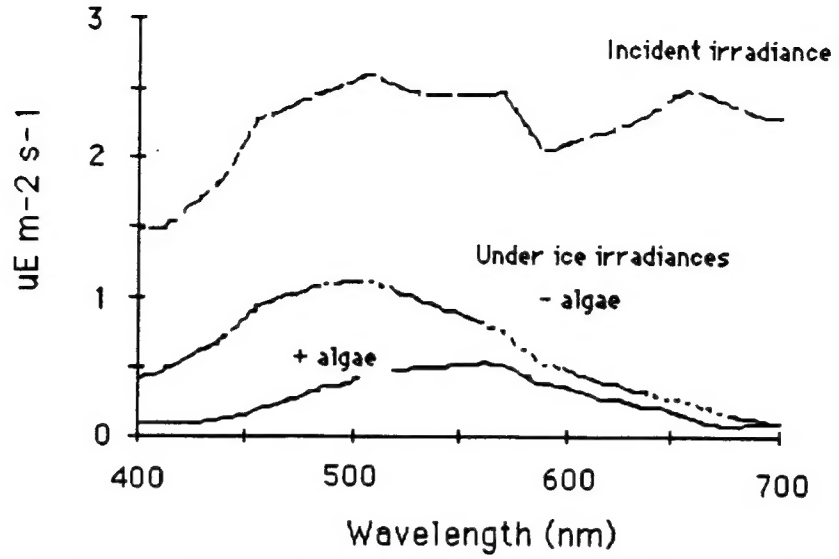

Figure 11. Downwelling spectral irradiance at the surface of the ice (measured on JD 99, 0800 hours), and predicted under ice downwelling spectral irradiances with and without 300 mg chla m^{-2}. Ice thickness = 1.2 meters, Snow depth = 0.001 meters.

Table I. Estimate of the partitioning of energy absorbed by sea ice, sea ice particulates and energy passing into the water column.

	Snow		Ice Layer #1			Ice Layer #2			H_2O	
	H	Z_1	E^p_{abs}	E^i_{abs}	Z_2	E^p_{abs}	E^i_{abs}			% E_{abs} by
Row #	(m)	(m)	(W m^{-2})	(W m^{-2})	(m)	(W m^{-2})	(W m^{-2})	(W m^{-2})		particles
1	0.01	1.2	10.6*	9.2	—	—	—	39.4		53.5
2	0.1	1.2	4.3*	2.5	—	—	—	13.5		55.1
3	0.2	1.2	1.6*	0.7	—	—	—	4.8		69.6
4	0.3	1.2	0.6*	0.2	—	—	—	1.0		75.0
5	0.01	1.2	0.0-	9.5	—	—	—	46.0		—
6	0.1	1.2	0.0-	2.7	—	—	—	16.0		—
7	0.3	1.2	0.0-	0.3	—	—	—	2.1		—
9	0.01	1.75	12.6*	10.3	0.4	3.8**	0.4	11.4		60.5
10	0.01	1.15	10.4*	9.0	0.05	9.6@	0.1	26.5		68.7
11	0.01	1.1	10.1*	8.8	0.1	16.7@	0.2	20.1		74.9

H = snow depth, Z_1 and Z_2 = depth of ice layer 1 and 2 respectively, E^x_{abs} = energy absorbed by constituent x, where p = particulate matter, and i = ice. The column headed by "H_2O" shows the amount of energy leaving the ice sheet and passing into the water column. % E_{abs} by particles is the percentage of the energy absorbed by the ice sheet which is absorbed by the particulate matter. Incident downwelling irradiance was set as that measured at 0800 hour on JD 99 (figure 2 and 11) (152 W m^{-2}).

* $ap(\lambda)$ set as the $\langle ap(\lambda) \rangle$ of the lead ice core L2 (figure 9).

- $ap(\lambda)$ set to zero at all wavelengths.

** $ap(\lambda)$ set as the $ap(\lambda)$ of the particulate matter collected from section C of the HH2 ice core (figure 7).

@ $ap(\lambda)$'s modeled as the chla specific absorption coefficient (m^2 mg $chla^{-1}$) of a congelation ice algal community[7] multiplied by the chlorophyll concentration in order to approximate the effect of a rich algal layer (300 mg m^{-2}) within the ice.[29] Figure 11 illustrates the predicted under ice irradiances with 300 mg chla m^{-2}.

4. DISCUSSION

It has been observed on several occasions that sediment-laden ice or algal assemblages within sea ice may induce premature ice melting and alter the physical structure of the sea ice and snow. Cryoconite holes, for example, are common in ice which has sediment deposits on its surface[25] and ablation of bottom ice occurs earliest where algal assemblages occur.[26] These phenomena are thought to be mediated through the selective absorption of EMR by the particulate matter and re-radiation of the absorbed energy as heat thus causing localized melting.

A single stream radiative transfer model applied to multiple layers indicates that particles were the major constituents absorbing EMR (400-700 nm) within the interior portions of sea ice. When detritus and/or minerals are more abundant than observed at "O" camp or when microalgal communities develop in the sea ice, they are predicted to have even more dramatic effects on the transfer of EMR into the sea ice and upper layers of the Arctic ocean. The prescence of a rich algal layer reduces and shifts the transmitted spectral irradiance from 500 nm to >550nm wavelengths (figure 11) (also see references 5,7, and 8). Furthermore, an ice sheet containing a rich algal layer in the bottom portions of the ice may increase the energy absorbed within the sea ice by 300 to 360% (table 1, rows 10 and 11).

Although the ice cores collected at "O" camp contained areas of visually apparent particulate matter, the majority of the ice volume appeared particle free. Yet, when the samples were analyzed microscopically and optically it was revealed that **all** layers along the sea iceprofile contained particulate matter which contributed to the inherent optical properties of the ice sheet. Multiple studies[25,28,28] indicate particle-laden sea ice in the Arctic basin is common and is a significant carrier for cross-shelf transport of sediments and continental shelf erosion.[28] The significance of particle-laden ice throughout the Arctic basin is that biogenic as well as nonbiogenic particulate matter may play a significant role in local radiative transfer and therefore biological (e.g. primary production) as well as physical processes including heat and energy transfer. Their effect will be most pronounced in areas where there is little snow, and turbid ice occurs due to sediment entrapment and/or microalgal community development within the ice matrix.

Since particulate material in sea ice is variable in both space and time, we can not yet determine quantitatively the role particulates have in determining the optical, thermal, and biological properties of Arctic sea ice. Further analysis of the factors controlling the spatial (both vertical and horizontal) and temporal distribution of terrigenous matter, aeolean particulates, detritus, and algae in sea ice seems warranted.

5. Acknowledgements

We thank S. F. Ackley for the use of a CRREL ice auger, K. Arrigo and D. Stramski for helpful discussions and comments, and the Office of Naval Research for support given to C . W. Sullivan under contract # N00014-88-0187 and R. Iturriaga under contract #N00014-89-J-1047.

7. REFERENCES

1. D. K. Perovich, "Theoretical estimates of light reflection and transmission by spatially complex and temporally varying sea ice covers," J. Geophys. Res., 95(C6): 9557-9567. 1990.

2. W. J. Wiscombe, and S. G. Warren, "A Model for the spectral albedo of snow. I: Pure snow," J. Atmos. Sci., 37: 2712-2733, 1980.

3. G. A. Maykut, and T. C. Grenfell, "The spectral distribution of light beneath first-year sea ice in the Arctic Ocean," Limnol. and Ocean., 20: 554-563, 1975.

4. A. C. Palmisano, J. B. SooHoo, R. L. Moe, and C. W. Sullivan, "Sea ice microbial communities. VII. Changes in under-ice spectral irradiance during the development of Antarctic sea ice microalgal communities," Mar. Ecol. Prog. Ser., 35: 165-173, 1987.

5. J. B. SooHoo, A. C. Palmisano, S. T. Kottmeier, M. P. Lizotte, S. L. SooHoo, and C. W. Sullivan, "Spectral Light absorption and quantum yield of photosynthesis in sea ice microalgae and a bloom of Phaeocystis pouchetii from McMurdo Sound, Antarctica," Mar. Eco. Prog. Ser., 35: 153-164, 1987.

6. T. E. Osterkamp, and J. P. Gosink, "Observations and analysis of sediment-laden sea ice," The Alaskan Beufort Sea, Ecosystems and Environments, P. W. Barnes, D. M. Schell, and R. Reimnitz (eds), pp. 73-93, Academic Press Inc., Orlando, Florida, 1984.

7. K. R. Arrigo, C. W. Sullivan, and J. N. Kremer, "A bio-optical model of Antarctica sea ice," J. Geophys. Res., 96(c6): 10,581-10592, 1990.

8. T. C. Grenfell, "A radiative transfer model for sea ice with vertical structure variations," J. Gophys. Res., 96(C9): 16,991-17,001, 1991.

9. T. C. Grenfell, "A Multi-layer radiative transfer model for the translucent geophysical surfaces with specific application to sea ice," SPIE vol. 1302 Ocean Optics X., 532-544. 1990.

10. G. A. Gilbert, and R. R. Buntzen, "In-situ measurements of the optical properties of arctic sea ice," SPIE vol. 637 Ocean Optics VIII., 252-263, 1986.

11. M. Kishino, C. R. Booth, and N. Okami, "Underwater radiant energy absorbed by phytoplankton, detritus, dissolved organic matter, and pure water" Limnol. Oceanogr., 29: 340-349, 1984.

12. K. S. Baker, and R. C. Smith, "Bio-optical classification and model of natural waters," Limnol. Oceanogr., 27(3): 500-509, 1982.

13. S. L. Sathyendranath, T. Platt, C. M. Caverhill, R. E. Warnock, and M. R. Lewis, "Remote sensing of oceanic primary production: computation using a spectral model," Deep-Sea Res., 36: 431-453,1989.

14. Grenfell, T. C. "A theoretical model of the optical properties of sea ice in the visible and near infrared," J. Geophys. Res., 88(C14): 9723-9735, 1983.

15. D. A. Kiefer, and J. B. SooHoo, "Spectral absorption by marine particles of coastal waters of Baja California," Limnol. Oceanogr., 27: 492-499, 1982.

16. B. G. Mitchell, and D. A. Kiefer, "Determination of absorption and fluorescence excitation spectra for light limited phytoplankton," Marine phytoplankton and productivity, O. Holm-Hansen et al.(eds), pp. 157-169. Springer, 1987.

17. R. Ituriaga, and D. A. Siegel, "Discrimination of the absorption properties of marine particulates using a microphotometric technique," SPIE vol. 925 Ocean Optics IX, 277-287, 1988.

18. R. Ituriaga, and D. A. Siegel. "Microphotometric characterization of phytoplankton and detrital absorption in the Sargasso Sea" Limnol. Oceanogr., 34: 1706-1726, 1989.

19. D. K. Perovich, personal communication, 1991.

20. S. G. Warren, "Optical properties of snow," Rev. Geophys. Space Phys., 20(1): 67-89, 1982.

21. D. T. Brine, and M. Iqbal, "Diffuse and global solar spectral irradiance under cloudless skies," Solar Energy., 30: 447-453, 1983.

22. T. C. Grenfell, and G. A. Maykut, "The optical properties of ice in the Arctic Basin," J. Glaciol., 18: 445-463, 1977.

23. A. Morel, and A. Bricaud, "Theoretical results concerning light absorption in a discrete medium, and application to specific absorption of phytoplankton," Deep-Sea Res., 28A: 1375-1393, 1981.

24. A. Bricaud, and D. Stramski, "Spectral absorption coefficients of living phytoplankton and nonalgal biogenous matter: A comparison between the Peru upwelling area and Sargasso Sea," Limnol. Oceanogr., 35(3): 562-582, 1990.

25. S. Pfirman, J. C. Gascard, I. Wollenburg and A. Abelmann, "Particle-laden Eurasian Arctic sea ice: observations from July and August 1987," Polar Res, 7(1): 313-315, 1989.

26. S. M. Grossi, S. T. Kottmeier, R. L. Moe, G. T. Taylor, and C. W. Sullivan, "Sea ice mocrobial communities. V. Growth and primary production in bottom ice under graded snow cover," Mar. Ecol. Prog. Ser., 35: 153-164, 1987.

27. B. B. Larssen, A. Elverhoi and P. AAgaard, "Study of particulate material in sea ice in the Fram Strait -a contribution to paleoclimatic research?" Polar Res., 5(3): 313-315, 1987.

28. P. W. Barnes, E. M. Kempema, and E. Reimnitz, "Source characteristics, and significance of sediment pellets formed on the sea ice of the Arctc Basin." in "Sea ice properties and processes: proceedings of the W. F. Weeks sea ice symposium," S. F. Aclkley and W. F. Weeks (eds), pp. 106-108, 1990.

29. H. E. Welch and M. A. Bergmann, "Seasonal development of ice algae and its prediction from environmental factors near resolute, N. W. T., Canada," Can. J. Fish. Aquat. Sci., 46: 1793-1804, 1990